

# THE RADIO SURFACE-BRIGHTNESS-TO-DIAMETER RELATION FOR GALACTIC SUPERNOVA REMNANTS: SAMPLE SELECTION AND ROBUST ANALYSIS WITH VARIOUS FITTING OFFSETS

M. PAVLOVIĆ<sup>1</sup>, D. UROŠEVIĆ<sup>1,2</sup>, B. VUKOTIĆ<sup>3</sup>, B. ARBUTINA<sup>1</sup>, AND Ü. D. GÖKER<sup>4</sup>

<sup>1</sup> Department of Astronomy, Faculty of Mathematics, University of Belgrade, Studentski trg 16, 11000 Belgrade, Serbia; marko@math.rs

<sup>2</sup> Isaac Newton Institute of Chile, Yugoslavia Branch

<sup>3</sup> Astronomical Observatory, Volgina 7, 11060 Belgrade 38, Serbia

<sup>4</sup> Physics Department, Boğaziçi University, Bebek 34342, Istanbul, Turkey

Received 2012 June 12; accepted 2012 October 16; published 2012 December 20

## ABSTRACT

In this paper, we present new empirical radio surface-brightness-to-diameter ( $\Sigma$ - $D$ ) relations for supernova remnants (SNRs) in our Galaxy. We also present new theoretical derivations of the  $\Sigma$ - $D$  relation based on equipartition or on a constant ratio between cosmic rays and magnetic field energy. A new calibration sample of 60 Galactic SNRs with independently determined distances is created. Instead of (standard) vertical regression, used in previous papers, different fitting procedures are applied to the calibration sample in the  $\log \Sigma$ - $\log D$  plane. Non-standard regressions are used to satisfy the requirement that values of parameters obtained from the fitting of  $\Sigma$ - $D$  and  $D$ - $\Sigma$  relations should be invariant within estimated uncertainties. We impose symmetry between  $\Sigma$ - $D$  and  $D$ - $\Sigma$  due to the existence of large scatter in both  $D$  and  $\Sigma$ . Using four fitting methods that treat  $\Sigma$  and  $D$  symmetrically, different  $\Sigma$ - $D$  slopes  $\beta$  are obtained for the calibration sample. Monte Carlo simulations verify that the slopes of the empirical  $\Sigma$ - $D$  relation should be determined by using orthogonal regression because of its good performance in data sets with severe scatter. The slope derived here ( $\beta = 4.8$ ) is significantly steeper than those derived in previous studies. This new slope is closer to the updated theoretically predicted surface-brightness-diameter slope in the radio range of the Sedov phase. We also analyze the empirical  $\Sigma$ - $D$  relations for SNRs in a dense environment of molecular clouds and for SNRs evolving in the lower-density interstellar medium. Applying new empirical relations to estimate distances of Galactic SNRs results in a dramatically changed distance scale.

*Key words:* ISM: supernova remnants – methods: analytical – methods: statistical – radio continuum: ISM

*Online-only material:* color figures

## 1. INTRODUCTION

Supernova remnants (SNRs) are the main sources of kinetic energy and heat for the interstellar medium (ISM). They also contribute to the acceleration of cosmic rays (CRs). The total number of Galactic SNRs is predicted to be between 1000 and 10,000 (Berkhuijsen 1984; Li et al. 1991; Tammann et al. 1994). Assuming a typical evolution timescale ( $\sim 10^5$  yr) of SNRs before they merge with the ISM and an event rate of two supernovae (SNe) per century in the Milky Way (Dragicevich et al. 1999),  $\sim 2000$  SNRs are expected in our Galaxy. However, just 274 SNRs have been identified in our Galaxy from their emission line spectra and radio and X-ray radiation (Green 2009). Such a great deficit points to the selection effects in past surveys. All known SNRs are sources of radio-synchrotron emission.

SNRs were often discovered in radio surveys of the Galactic plane. Because of the surface-brightness limit of previous surveys, more faint or confused SNRs await discovery. The dominant selection effects are those that are applicable at radio wavelengths. To put it simply, three selection effects apply to the identification of Galactic SNRs (e.g., Green 1991): (1) difficulty in identifying faint remnants, (2) difficulty in identifying small angular size remnants, and (3) the absence of uniform coverage of the sky. Additionally, Malmquist bias<sup>5</sup> is severe in the Galactic samples, making them incomplete. In the case of extragalactic SNRs, the selection effects are different (see Urošević et al. 2005).

The important and very difficult task of determining distances to Galactic SNRs is often based on observations in the radio do-

main. It is possible to determine direct distances from historical records of SNe; proper motions and radial velocities; kinematic observations; coincidences with H I, H II, and molecular clouds; and OB associations and pulsars (Green 1984). Where direct distance determination is not possible, estimates can be made for shell SNRs using the radio surface-brightness-diameter relationship ( $\Sigma$ - $D$ ). The mean surface brightness at a specific radio frequency,  $\Sigma_\nu$ , is a distance-independent parameter and is an important characteristic of an SNR (Shklovsky 1960a). The radio surface brightness at frequency  $\nu$  to diameter relation for SNRs has been written in general form as

$$\Sigma_\nu(D) = AD^{-\beta}, \quad (1)$$

where  $A$  depends on the properties of the SN explosion and ISM, such as the SN energy of explosion, the mass of the ejected matter, the density of the ISM, the magnetic field strength, etc., while  $\beta$  is thought to be independent of these properties (Arbutina & Urošević 2005). For empirical relations, parameters  $A$  and  $\beta$  are obtained by fitting the data for a sample of SNRs of known distances.

According to the existing convention, SNRs are classified into three basic types: shell remnants, plerionic or filled-center remnants, and composite remnants. Allakhverdiyev et al. (1983a, 1983b, 1986a, 1986b) showed that the  $\Sigma$ - $D$  relation is only applicable to shell-type SNRs. However, it can also be used for composite remnants if we separate the flux from the surrounding shell and the central regions.

The first theoretical  $\Sigma$ - $D$  relation was derived by Shklovsky (1960a). He was also the first to propose the use of this relation as a method for determining SNR distances (Shklovsky 1960b). An updated theoretical derivation of this relation for

<sup>5</sup> The volume selection effect: brighter objects are favored in flux density limited surveys.

shell-like SNRs was made by Berezhko & Völk (2004). The first empirical relations were derived by Poveda & Woltjer (1968), Milne (1970, 1979), Clark & Caswell (1976), and many other authors. An important Galactic relation frequently used in the last decade was derived by Case & Bhattacharya (1998, hereafter CB98). The updated Galactic  $\Sigma$ - $D$  relation was derived by Guseinov et al. (2003), Xu et al. (2005), and Stupar et al. (2007). More than five decades after the first published study of the relation, it continues to evolve both in theoretical and empirical aspects. A detailed review of Galactic and extragalactic empirical  $\Sigma$ - $D$  relations was presented by Urošević (2002).

Although many authors have improved the theoretical and empirical  $\Sigma$ - $D$  relations, there are still some doubts about when this relation should be applied to determine distances to individual remnants. Green (1984) presented a critical analysis, noting that remnants with reliable distances have widespread intrinsic properties leading to significant dispersion in the  $\Sigma$ - $D$  diagram. One of the main problems is the high level of uncertainty for independently determined distances of SNRs, which are used for  $\Sigma$ - $D$  calibration. Also, a variety of selection effects may be present in the data samples of both Galactic and extragalactic SNRs. Arbutina et al. (2004) concluded that evolutionary paths may differ from remnant to remnant because of the potentially wide range of intrinsic properties of SN explosions (and progenitor stars) and the ISM into which they expand. Arbutina & Urošević (2005) showed that different  $\Sigma$ - $D$  relations can be constructed for two different samples, remnants in a dense environment of molecular clouds and SNRs evolving in ISM of lower density.

A similar relation can also be used for composite SNRs, but few of those remnants have known distances, and it is difficult to obtain a  $\Sigma$ - $D$  relation for them. The  $\Sigma$ - $D$  relation is often the only method for distance determination for shell SNRs. Despite the inherent uncertainties and assumptions of this method, we suggest that the often-used  $\Sigma$ - $D$  relation by CB98 should be updated because of the significant increase in the number of SNR calibrators. Additionally, different fitting procedures have to be used for establishing proper  $\Sigma$ - $D$  calibration; we emphasize that in all previous papers the standard fitting procedure, based on vertical (parallel to  $y$ -axes)  $\chi^2$  regression, was being used to derive empirical  $\Sigma$ - $D$  relations for the Galactic SNR samples (e.g., Poveda & Woltjer 1968; Clark & Caswell 1976; Milne 1979; CB98; Guseinov et al. 2003; Xu et al. 2005). In this paper, we select calibrators from Green’s SNR catalog (Green 2009) based on literature up to the end of 2008.<sup>6</sup>

The  $\Sigma$ - $D$  relation has two particular uses: the derivation of diameters (and hence distances) and the parameterization of the relationship between surface brightness and diameter for comparison with models and theories. For the former, the measured value of  $\Sigma$  is used to predict  $D$ , and for this case a least-squares fit minimizing the deviations in  $\log D$  should be used. However, Urošević et al. (2010) suggested the use of the orthogonal regression fitting procedure for obtaining the empirical  $\Sigma$ - $D$  relation, instead of the classical vertical regression. Isobe et al. (1990) show that regression in astrophysical applications is more complex than most realize and give alternatives to ordinary vertical regression. In our paper, following the conclusions of Isobe et al. (1990), Green (2005), and Urošević et al. (2010), we test four different linear regression

methods (including already mentioned orthogonal regression) that treat variables  $\Sigma$  and  $D$  symmetrically. Symmetry between  $\Sigma$ - $D$  and  $D$ - $\Sigma$  is also required due to the existence of large scatter in both  $D$  and  $\Sigma$  axes. Therefore, the values of parameters obtained by fitting  $\Sigma$ - $D$  and  $D$ - $\Sigma$  relations have to agree within estimated uncertainties.

This paper also considers possible dependence of radio luminosity on the linear diameter ( $L$ - $D$  dependence). This criterion, established by Arbutina et al. (2004), is as follows: if the  $L$ - $D$  relation is obtained then the  $\Sigma$ - $D$  relation follows and it may be used for the estimation of SNR distances.

In Section 2, we present a new theoretical derivation of the  $\Sigma$ - $D$  relation based on equipartition between CRs and magnetic field energy.<sup>7</sup> The equations derived here describe three consecutive phases of the adiabatic (Sedov) phase of evolution of non-thermal radiation from SNRs. In Section 3, using the 274 SNRs in Green’s present catalog (2009 March version), we construct a calibration sample containing 60 Galactic shell remnants with distance estimates and use it to derive  $\Sigma$ - $D$  relation. Monte Carlo simulations are performed in Section 4 to estimate the influence of data scatter on the  $\Sigma$ - $D$  and  $L$ - $D$  slopes. In this section, we also derive the empirical Galactic  $\Sigma$ - $D$  relation of the calibration sample containing 60 SNRs. In Section 5, we apply our Galactic  $\Sigma$ - $D$  relation to obtain the distances of two newly discovered large and faint SNRs, G25.1-2.3 and G178.2-4.2. In Section 6, we present  $\Sigma$ - $D$  relations of a subsample of 28 Galactic SNRs evolving in dense environments and a subsample only 5 Galactic SNRs evolving in low density. In Section 7, we briefly review selection effects that influence Galactic samples of SNRs severely. The conclusions of this paper are presented in the last section.

## 2. A THEORETICAL INTERPRETATION OF THE $\Sigma$ - $D$ RELATION

A slightly different theoretical interpretation of the  $\Sigma$ - $D$  relation is presented for non-thermal radiation from SNRs. This model is based on equipartition introduced by Reynolds & Chevalier (1981). Equipartition is a useful tool for estimating magnetic field strength and the energy contained in the magnetic field and CR particles using only the radio-synchrotron emission of a source. Details of equipartition and revised equipartition calculations for radio sources in general are available in Pacholczyk (1970) and Govoni & Feretti (2004), and Beck & Krause (2005), respectively. Arbutina et al. (2012) introduced new modifications in equipartition calculation. They integrated over momentum to obtain energy densities of particles so there is no need to either introduce a break in the energy spectrum or take into account different ion species.

The total energy density of CRs can be written as the sum of two components (Arbutina et al. 2012): energy of electrons ( $\epsilon_e$ ) and ions ( $\epsilon_{\text{ion}}$ ):

$$\begin{aligned} \epsilon_{\text{CR}} = \epsilon_e + \epsilon_{\text{ion}} \approx \kappa K_e (m_e c^2)^{2-\gamma} \\ \times \left[ \frac{1}{\sum_i Z_i v_i} \left( \frac{m_p}{m_e} \right)^{2-\gamma} \cdot \left( \frac{2m_p c^2 E_{\text{inj}}}{E_{\text{inj}}^2 + 2m_e c^2 E_{\text{inj}}} \right)^{(\gamma-1)/2} \right. \\ \left. \cdot \frac{\Gamma\left(\frac{3-\gamma}{2}\right) \Gamma\left(\frac{\gamma-2}{2}\right)}{2\sqrt{\pi}(\gamma-1)} \sum_i A_i^{(3-\gamma)/2} v_i \right], \end{aligned} \quad (2)$$

<sup>6</sup> A Catalogue of Galactic Supernova Remnants (2009 March version), Astrophysics Group, Cavendish Laboratory, Cambridge, United Kingdom (also available on the Web at <http://www.mrao.cam.ac.uk/surveys/snrs/>).

<sup>7</sup> By “equipartition” we do not assume that the energies are necessarily equal or nearly equal, but rather that the energy ratio is constant during evolution.

where  $\gamma$  is the energy spectral index ( $2 < \gamma < 3$ ),  $E_{\text{inj}}$  is the injection energy of particles,  $m_e$  and  $m_p$  are electron and proton masses,  $v_i = n_i/n$  are ion abundances,  $A_i$  and  $Z_i$  are mass and charge numbers of elements, and  $K_e$  is the constant in the power-law energy distribution for electrons.  $\kappa$  is a slowly varying function (if  $E_{\text{inj}}$  is not very high; see Figure 2 in Arbutina et al. 2012) that incorporates the ratio between electron and ion energy (the latter of which should be dominant). Here, the term “total energy density” implies that we take into account all CR species (e.g., electrons, protons,  $\alpha$ -particles, and heavier ions) inside the SNR, which have been injected into the acceleration process. We neglect energy losses.

We assume that an isotropic power-law distribution of ultra-relativistic electrons is created at the shock wave (Bell 1978):

$$N(E)dE = K_e E^{-\gamma} dE. \quad (3)$$

For a given element of gas,  $K_e$  evolves behind the shock wave as a result of the conservation of energy. The flux density of synchrotron radiation of ultrarelativistic electrons, obtained from Pacholczyk (1970) after substituting the emission coefficient  $\varepsilon_\nu$  with flux density  $S_\nu$ , is

$$S_\nu \propto K_e B^{1+\alpha} V \nu^{-\alpha} \text{ W m}^{-2} \text{ Hz}^{-1}, \quad (4)$$

where  $B$  is the magnetic field strength,  $V$  is the volume,  $\nu$  is the frequency, and  $\alpha$  is the synchrotron spectral index defined as  $\alpha = (\gamma - 1)/2$ . Here, we use the flux density defined as

$$S_\nu = \frac{L_\nu}{4\pi d^2} = \frac{\varepsilon_\nu V}{d^2} = \frac{4\pi}{3} \varepsilon_\nu f \theta^3 d, \quad (5)$$

where  $L_\nu$  is the radio luminosity,  $f$  is the volume filling factor of radio emission,  $d$  is the distance, and  $\theta = R/d$  is the angular radius. Then, we obtain the  $\Sigma$ – $D$  relation

$$\Sigma_\nu = A D^{-\beta} = \frac{L_\nu}{\pi^2 D^2} \propto S_\nu D^{-2} \text{ W m}^{-2} \text{ Hz}^{-1} \text{ sr}^{-1}. \quad (6)$$

$\Sigma_\nu$  represents surface brightness defined as  $\Sigma_\nu = S_\nu/\Omega$ , where  $\Omega$  (in steradians) is the solid angle of the radio source.

Reynolds & Chevalier (1981) assumed a redistribution of energy between CRs, the magnetic field, and thermal gas behind shock wave (equipartition between  $\epsilon_{\text{CR}}$  and  $\epsilon_B$ ) described as

$$\epsilon_{\text{CR}} \approx \epsilon_B = \frac{1}{2\mu_0} B^2 \propto \rho_0 v_s^2, \quad (7)$$

where  $v_s$  is the pre-shock velocity and  $\rho_0$  is the pre-shock ambient density. We introduce the parameter  $s$  to allow for an ambient density profile of the form  $\rho \propto R^{-s}$ ,  $R \propto t^m$ , and  $\gamma = 2\alpha + 1$ , where  $R$  represents radius ( $D = 2R$ ) and  $m$  is known as a deceleration parameter (Bandiera & Petruk 2004). This relation also contains a break, similar to the relation of Duric & Seaquist (1986).

If we assume low shock velocity (older SNRs) so that  $E_{\text{inj}} = m_p v_s^2 \ll 2m_e c^2$ , i.e.,  $v_s \ll 7000 \text{ km s}^{-1}$ , from Equation (2), we have

$$K_e \propto \rho_0 v_s^2, \quad (8)$$

and, after expressing  $B \propto (\rho_0 v_s^2)^{1/2}$  from Equation (7) and inserting  $V \propto D^3$ , with  $v_s = (dR/dt) \propto m t^{m-1} \propto m D^{m-1/m}$  we find the relation

$$S_\nu \propto K_e \frac{\nu^{+\frac{5}{4}}}{4} V \propto (\rho_0 v_s^2)^{\frac{\gamma+5}{4}} D^3 \propto D^{\left(\frac{2(m-1)}{m}-s\right)\frac{\alpha+3}{2}+3}. \quad (9)$$

Taking  $s = 0$  and  $m = 2/5$  (Sedov 1959) leads to

$$\Sigma_\nu \propto D^{-\frac{3\alpha+7}{2}}, \quad (10)$$

and substituting an average SNR spectral index  $\alpha = 0.5$  gives  $\beta = 17/4 = 4.25$  (see Reynolds & Chevalier 1981; Berezhko & Völk 2004).

Another possibility is  $E_{\text{inj}} \gg 2m_e c^2$ , i.e.,  $v_s \gg 7000 \text{ km s}^{-1}$ , which is satisfied for younger remnants. In this case, following Equation (2), constant  $K_e$  in the power-law energy distribution of electrons has the form

$$K_e \propto \rho_0 v_s^2 E_{\text{inj}}^{\frac{\gamma-1}{2}} \propto \rho_0 v_s^{2(\alpha+1)}, \quad (11)$$

and therefore the flux density is

$$S_\nu \propto \rho_0^{\frac{\alpha+3}{2}} v_s^{3(\alpha+1)} D^3 \propto D^{\frac{3(\alpha+1)(m-1)}{m} - \frac{s(\alpha+3)}{2} + 3}. \quad (12)$$

Taking  $s = 0$  and  $m = 2/5$  yields

$$\Sigma_\nu \propto D^{-\frac{9\alpha+7}{2}}, \quad (13)$$

and substituting  $\alpha = 0.5$  gives  $\beta = 23/4 = 5.75$ .

Berezhko & Völk (2004) applied time-dependent nonlinear kinetic theory for CR acceleration in SNRs in studying the properties of the synchrotron emission. In particular, they applied detailed numerical calculations for deriving the surface-brightness–diameter ( $\Sigma$ – $D$ ) relation for the range of relevant physical parameters, namely ambient density ( $n_{\text{H}}$ ) and SN explosion energy ( $E_{\text{sn}}$ ). Berezhko & Völk (2004) derived  $\Sigma$ – $D$  relations for different phases of SNR evolution.

During the initial part of the free expansion phase, the expected dependence is

$$\Sigma_\nu \propto n_{\text{H}}^{7/4} D, \quad (14)$$

which explains well the numerical  $\Sigma_\nu(D)$  behavior of small  $D$ . In this region,  $\Sigma_\nu(D)$  does not depend on the SN parameters  $E_{\text{sn}}$  and  $M_{\text{ej}}$  (mass of ejected matter), but it does depend on the ISM density.

During the later part of the free expansion phase, the expected dependence is

$$\Sigma_\nu \propto (E_{\text{sn}}/M_{\text{ej}})^{7/16} n_{\text{H}}^{21/16} D^{-5/16}. \quad (15)$$

In the subsequent Sedov<sup>8</sup> phase, we have

$$\Sigma_\nu \propto E_{\text{sn}}^{7/14} D^{-17/4}, \quad (16)$$

independent of  $n_{\text{H}}$  and  $M_{\text{ej}}$ .

In the late Sedov phase, dependence goes toward

$$\Sigma_\nu \propto E_{\text{sn}} n_{\text{H}}^{3/4} D^{-2}. \quad (17)$$

We note that the phase described by Equation (13), based on equipartition, represents an additional intermediate phase between the late free expansion and early Sedov phases introduced by Berezhko & Völk (2004). Therefore, Equations (13), (16), and (17) respectively describe three consecutive phases of the adiabatic (Sedov) phase of evolution of SNRs. SNRs spend most of their evolution in the Sedov phase, up to almost a million years

<sup>8</sup> Also known as Sedov–Taylor phase.

in a hot ISM (McKee & Ostriker 1977). Usually, pressure effects are responsible for terminating the Sedov phase earlier.

Based on previous results and assuming that the majority of SNRs are in the Sedov phase, we expect to obtain  $\Sigma$ - $D$  slope  $\beta$  in the range of 2–5.75, depending on the evolutionary stage of the remnants in a sample of shell-type SNRs. Also, we should expect additional scatter (which does not affect the slope significantly) in the  $\Sigma$ - $D$  diagram due to different properties of the SN explosion and ISM, such as the energy of explosion, the mass of the ejected matter, and the density of the ISM.

### 3. CALIBRATION SAMPLE AND NEW $\Sigma$ - $D$ RELATION

To obtain a reliable empirical  $\Sigma$ - $D$  relation, we used a sample of shell-type SNRs with independently determined distances and well-determined angular diameters and flux densities. Various methods provide distance estimates to the remnants such as proper motions; shock and radial velocities; H I absorption and polarization; association or interaction with H I, H II, and CO molecular clouds; X-ray observations; optical extinction; and low frequency radio absorption. Of the 274 SNRs in Green’s present catalog (2009 March version), 84 have independently determined distances (59 of them classified as shell type, 14 composite, 6 filled center, and 5 unknown type). The flux densities given in the catalog and the calculated surface brightnesses in this paper are referenced to 1 GHz.

The surface brightnesses and angular diameters are taken from Green’s catalog. This catalog was also our primary source of information about the distances of remnants. Many of the SNRs from this catalog have more than one distance available. Following the CB98 approach, we have either chosen the most recent measurement or used an average of the available estimates (if the given distance range is narrow enough). We have also searched the literature for recent papers not included in Green’s catalog, which provide accurate distances to Galactic shell remnants. Our Galactic sample of 60 shell remnants with direct distance estimates, which is used to derive new  $\Sigma$ - $D$  relations, is listed in Table 1.

Part of our Galactic sample contains 33 SNRs, with updated parameters, which were also used as calibrators by CB98. The following four SNRs from the CB98 sample were omitted from our sample. According to Green’s catalog, the shell structure, as well as the flux density at 1 GHz, of G49.2–0.7 (W51) is questionable, while G330.0+15.0 (Lupus Loop) does not have enough accurate measurements of angular diameter and flux density. Up to now, only a lower limit for the distance of remnant G304.6+0.1 (Kes 17) has been measured (9.7 kpc from H I absorption). Foster et al. (2006) showed that OA 184, previously classified as SNR G166.2+2.5, is actually a Galactic H II region energized by O7.5V star BD+41°1144.

Our Galactic sample also includes five composite SNRs because (1) they have a pure shell structure in radio regardless of centrally brightened radio morphology or (2) it was possible to separate the shell flux density from the pulsar wind nebula (PWN) flux density. Tam et al. (2002) determined the integrated flux over various regions in the composite source G11.2–0.3. From their measurements and integrated flux density measurements of G11.2–0.3 at different frequencies, we estimate the SNR shell flux density at 1 GHz to be 20.5 Jy (subtracting PWN flux density, which represents about 3% of the flux density of the entire source). G93.3+6.9 (DA 530) is a high Galactic latitude SNR with a well-defined shell-like radio morphology that has a centrally filled morphology only in X-rays (Jiang et al 2007).

Observed in radio, the composite SNR G189.1+3.0 (IC 443) consists of two connected, roughly spherical shells of radio-synchrotron emission that are centered at different locations. Combining their measurements with existing data, Castelletti et al. (2011a) estimated that the flux density of the PWN represents only about 0.1% of the total flux density and therefore we calculated the SNR shell flux density at 1 GHz to be 164.7 Jy. Castelletti et al. (2011b) investigated in detail the radio emission belonging to SNR G338.3–0.0 around the X-ray pulsar candidate in a search for traces of a PWN, by reprocessing data corresponding to observations acquired with the Australia Telescope Compact Array (ATCA).<sup>9</sup> No nebular radio emission has been found to correspond to the X-ray PWN, in spite of the good quality of their radio images down to low surface-brightness limits, and therefore the measured flux density in radio corresponds only to the SNR shell flux density. Based on the radio images and the comparison of X-ray and IR observations, Giacani et al. (2011) confirmed that there is no PWN within composite remnant G344.7–0.1. Also, the same authors redetermined the distance of this SNR to be  $(6.3 \pm 0.1)$  kpc on the basis of H I absorption and emission.

The shell remnant G1.9+0.3 is the youngest known Galactic SNR with known distance and the only Galactic SNR increasing in flux. Its estimated age is  $156 \pm 11$  yr (Carlton et al. 2011) and its distance is about 8.5 kpc. Therefore, this SNR should not be included in our sample because it is probably still in the phase of free expansion.

We mentioned in Section 1 that in the past a single linear regression method was used for the purpose of obtaining the empirical  $\Sigma$ - $D$  relation: ordinary least-squares regression of the dependent variable  $Y$  against independent variable  $X$ , or OLS( $Y|X$ ).<sup>10</sup> In OLS( $Y|X$ ), the regression line is defined as that which minimizes the sum of the squares of the  $Y$  residuals. Some applications, however, require using alternatives to OLS( $Y|X$ ). The class of alternatives to OLS( $Y|X$ ) used in our paper was suggested by Isobe et al. (1990) for problems where the intrinsic scatter of data dominates any errors arising from the measurement process. This class of methods has also been proposed in order to avoid specifying “independent” and “dependent” variables.

The most important purpose of the  $\Sigma$ - $D$  relation is to estimate diameters (and hence distances) for Galactic SNRs based on their observed surface brightnesses. Green (2005) also stated an important issue related to the  $\Sigma$ - $D$  fits, even when disregarding problems with the selection effects. Namely, he pointed out that the measured value of  $\Sigma$  is used to predict  $D$ , and that a least-squares fit minimizing the deviations in  $\log D$  should be used to that effect. This, however, has not been done thus far, and fits minimizing the deviations in  $\log \Sigma$  have been used instead. He also mentioned that a fit to data that treats  $\Sigma$  and  $D$  symmetrically is appropriate if a  $\Sigma \propto D^n$  relation is used to describe the relationship between  $\Sigma$  and  $D$  and, by extension, the radio evolution of SNRs.

Four methods that treat the variables symmetrically have been suggested by Isobe et al. (1990). One is the line that bisects the OLS( $Y|X$ ) and the inverse OLS( $X|Y$ ) lines, called the “OLS bisector” or “double regression,” which has been applied in characterization of the Tully–Fisher and Faber–Jackson relations to estimate galaxy distances (Rubin et al. 1980; Lynden-Bell et al. 1988; Pierce & Tully 1988). The second

<sup>9</sup> The ATCA is an array of six 22 m antennas used for radio astronomy.

<sup>10</sup> Notation introduced by Isobe et al. (1990).

**Table 1**  
Shell SNRs with Known Distances<sup>a</sup>

Catalog Name	Other Name	Surface Brightness (W m <sup>-2</sup> Hz <sup>-1</sup> sr <sup>-1</sup> )	Distance (kpc)	Diameter (pc)	Reference
G4.5+6.8 <sup>b</sup>	Kepler, SN1604, 3C358	3.18e-19	6.0	5.2	1
G11.2-0.3		1.93e-19	4.4	5.1	7
G18.8+0.3 <sup>b</sup>	Kes 67	2.66e-20	12.0	47.7	2
G21.8-0.6	Kes 69	2.60e-20	5.2	30.3	3
G23.3-0.3	W41	1.45e-20	4.2	33.0	2
G27.4+0.4	Kes 73, 4C-04.71	5.64e-20	8.65	10.1	2
G31.9+0.0 <sup>b</sup>	3C391	1.03e-19	8.5	14.6	2
G33.6+0.1 <sup>b</sup>	Kes 79	3.31e-20	7.0	20.4	4
G41.1-0.3	3C397	2.94e-19	10.3	10.0	5
G43.3-0.2 <sup>b</sup>	W49B	4.77e-19	10.0	10.1	2
G46.8-0.3 <sup>b</sup>	HC30	9.53e-21	7.8	33.7	2
G53.6-2.2 <sup>b</sup>	3C400.2, NRAO 611	1.30e-21	2.8	24.8	2
G54.4-0.3 <sup>b</sup>	HC40	2.63e-21	3.3	38.4	6, 7
G55.0+0.3		2.51e-22	14.0	70.5	2
G65.1+0.6		1.84e-22	9.0	175.6	2
G74.0-8.5 <sup>b</sup>	Cygnus Loop	8.59e-22	0.54	30.1	8
G78.2+2.1 <sup>b</sup>	γ Cygni, DR4	1.34e-20	1.20	20.9	9
G84.2-0.8 <sup>b</sup>		5.17e-21	4.50	23.4	7, 10
G89.0+4.7 <sup>b</sup>	HB21	3.07e-21	0.8	24.2	2
G93.3+6.9	DA 530, 4C(T)55.38.1	2.51e-21	2.2	14.9	7
G93.7-0.2	CTB 104A, DA 551	1.53e-21	1.5	34.9	2
G94.0+1.0	3C434.1	2.61e-21	5.2	41.4	2
G96.0+2.0		6.68e-23	4.0	30.3	2
G108.2-0.6		3.19e-22	3.2	57.2	2
G109.1-1.0	CTB 109	4.22e-21	3.2	26.1	11
G111.7-2.1 <sup>b</sup>	Cassiopeia A, 3C461	1.64e-17	3.4	4.9	2
G114.3+0.3		1.67e-22	0.7	14.3	2
G116.5+1.1 <sup>b</sup>		3.14e-22	1.6	32.2	2
G116.9+0.2 <sup>b</sup>	CTB 1	1.04e-21	1.6	15.8	2
G119.5+10.2 <sup>b</sup>	CTA 1	6.69e-22	1.4	36.7	2
G120.1+1.4 <sup>b</sup>	Tycho, 3C10, SN1572	1.32e-19	4.0	9.3	12
G127.1+0.5	R5	8.92e-22	1.25	16.4	2
G132.7+1.3 <sup>b</sup>	HB3	1.06e-21	2.2	51.2	2
G156.2+5.7 <sup>b</sup>		6.22e-23	1.0	32.0	13
G160.9+2.6 <sup>b</sup>	HB9	9.85e-22	0.8	30.2	14
G166.0+4.3 <sup>b</sup>	VRO 42.05.01	5.47e-22	4.5	57.4	2
G180.0-1.7	S147	3.02e-22	0.62	32.5	2
G189.1+3.0	IC443, 3C157	1.22E-20	1.5	19.6	7
G205.5+0.5 <sup>b</sup>	Monoceros Nebula	4.98e-22	1.2	76.8	2
G260.4-3.4 <sup>b</sup>	Puppis A, MSH 08-44	6.52e-21	2.2	35.1	2
G290.1-0.8	MSH 11-61A	2.38e-20	7.0	33.2	2
G292.2-0.5		3.51e-21	8.4	42.3	2
G296.5+10.0 <sup>b</sup>	PKS 1209-51/52	1.23e-21	2.1	46.7	15
G296.8-0.3	1156-62	4.84e-21	9.6	46.7	2
G309.8+0.0 <sup>b</sup>		5.39e-21	3.6	22.8	7
G315.4-2.3 <sup>b</sup>	RCW 86, MSH 14-63	4.18e-21	2.3	28.1	2
G327.4+0.4	Kes 27	1.02e-20	4.85	29.6	2
G327.6+14.6 <sup>b</sup>	SN1006, PKS 1459-41	3.18e-21	2.2	19.2	2
G332.4-0.4 <sup>b</sup>	RCW 103	4.21e-20	3.1	9.0	2
G337.0-0.1	CTB 33	1.34e-19	11.0	4.2	2
G337.8-0.1	Kes 41	5.02e-20	11.0	23.5	2
G338.3-0.0		1.57e-20	11.0	25.6	20
G340.6+0.3		2.09e-20	15.0	26.2	2
G344.7-0.1		3.76e-21	6.3	18.3	19
G346.6-0.2		1.88E-20	11.0	25.6	16
G348.5+0.1 <sup>b</sup>	CTB 37A	4.82e-20	7.9	34.5	21
G348.5+0.1 <sup>b</sup>	CTB 37B	1.35e-20	13.2	65.3	21
G349.7+0.2 <sup>b</sup>		6.02e-19	18.4	12.0	2
G352.7-0.1		1.25e-20	7.5	15.1	4
G359.1-0.5 <sup>b</sup>		3.66e-21	7.6	53.1	17, 18

**Notes.**

<sup>a</sup> Direct distance estimates, which can be inferred from proper motions, shock, and radial velocities; H I absorption and polarization; association or interaction with H I, H II, and CO molecular clouds; OB associations; pulsars; X-ray observations; optical extinction; and low frequency radio absorption.

<sup>b</sup> SNRs also belonging to Case & Bhattacharya's (1998) calibration sample.

**References.** (1) Chiotellis et al. 2012; (2) Green 2009; (3) Zhou et al. 2009; (4) Giacani et al. 2009; (5) Jiang et al. 2010; (6) Junkes et al. 1992; (7) Case & Bhattacharya 1998; (8) Blair et al. 2005; (9) Uchiyama et al. 2002; (10) Feldt & Green 1993; (11) Kothes & Foster 2012; (12) Asami Hayato et al. 2010; (13) Xu et al. 2007; (14) Leahy & Tian 2007; (15) Giacani et al. 2000; (16) Hewitt et al. 2009; (17) Uchida et al. 1992a; (18) Uchida et al. 1992b; (19) Giacani et al. 2011; (20) Castelletti et al. 2011b; (21) Tian & Leahy 2012.

**Table 2**  
The  $\Sigma$ - $D$  Fit Parameters for a Calibration Sample of 60 Galactic SNRs and Different Regression Methods

Fit	$\beta$	$\Delta\beta$	$\log A$	$\Delta\log A$	Average Fractional Error
OLS( $Y X$ )	2.2840	0.3282	-17.0028	0.4895	0.824
OLS( $X Y$ )	5.0375	0.7465	-13.1820	1.0162	0.469
Orthogonal	4.8161	0.7218	-13.4877	0.9819	0.472
Bisector	3.1741	0.3335	-15.7641	0.4746	0.575
Arithmetic mean	3.7079	0.4282	-15.0209	0.5817	0.522
Geometric mean	3.4178	0.3536	-15.4256	0.4898	0.547

**Note.** We give  $\beta$  and  $A$  in relation  $\Sigma_\nu = AD^{-\beta}$  as well as their errors.

method is the geometric mean of OLS( $Y|X$ ) and the OLS( $X|Y$ ) slopes, proposed as the “impartial” regression by Strömberg (1940) and used in cosmic distance scale applications. It was also independently derived by statisticians and called the “reduced major-axis.” The third regression is the line that minimizes the sum of the squares of the perpendicular distances between the data points and the line, often called “orthogonal regression” or “major-axis” regression. Urošević et al. (2010) applied orthogonal regression, for the first time, to obtain the empirical relation of SNRs in the starburst galaxy M82. The fourth method that treats the variables symmetrically represents the arithmetic mean of the OLS( $Y|X$ ) and OLS( $X|Y$ ) slopes (Aaronson et al. 1986). It is easily recognized that these four techniques, though each is invariant to switching variables (referred to as the dependent and independent), lead to completely different regression lines, both mathematically and in real applications.

The empirical  $\Sigma$ - $D$  relation depends greatly on the regression method adopted. The dispersion of the six estimates is considerably larger than the variance of any one estimate (see Table 2). For problems like these, Isobe et al. (1990) suggest calculating all six<sup>11</sup> regressions and being appropriately cautious regarding the confidence of the inferred conclusion. Accordingly, we give all mentioned regressions in Figure 1 (except OLS( $X|Y$ ), which is very close to orthogonal regression) that applied to our calibration sample of 60 shell SNRs.

Data fitting is performed analytically and by using bootstrap. The fit parameter values and their errors, presented in Table 2, were obtained after  $10^6$  bootstrap data re-samplings for each fit. After applying bootstrap, we obtain the distribution of a selected value for a certain regression procedure and then fit this dependence in OriginPro 8 with Gauss (normal) distribution, by using four-parameter fitting without parameter fixing. A normal distribution is used here as a good approximation to describe the behavior of bootstrap re-samples. Thus, we get a mean (expectation) and associated standard deviation for each parameter.

## 4. MONTE CARLO SIMULATIONS

### 4.1. $\Sigma$ - $D$ Relation

At first glance, an inspection of Figure 1 and Table 2 leads to the conclusion that the resulting fit parameter values are significantly influenced by the type of fitting procedure. This is mainly due to the large dispersion in the sample of calibrators

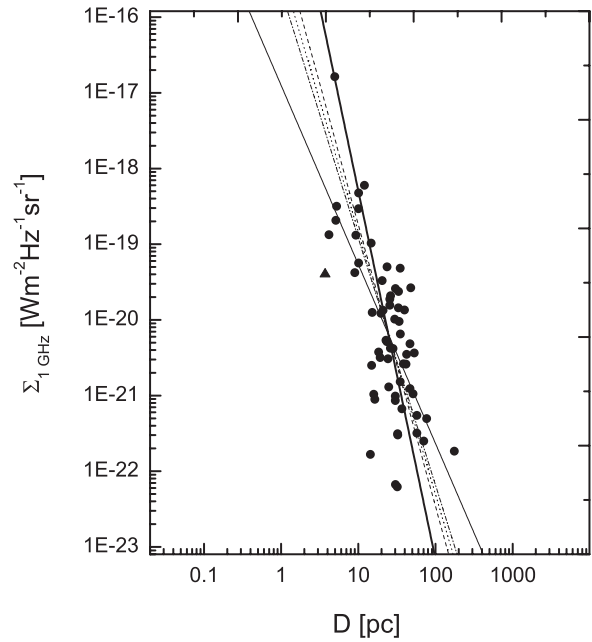


**Figure 1.** Surface brightness vs. diameter  $\Sigma$ - $D$  relation at 1 GHz for shell SNRs obtained by using the distance calibrators in Table 1. The different methods for minimizing the distance of the data from a fitted line are presented. The two solid lines represent OLS( $Y|X$ ) (thin line) and orthogonal regression (thick line). Dashed, dotted, and dash-dotted lines represent the arithmetic and geometric means of the OLS( $Y|X$ ) and OLS( $X|Y$ ) slopes and the OLS bisector, respectively. OLS( $X|Y$ ) line, with a slope very similar to orthogonal regression, is omitted to avoid complicating the graph. G1.9 + 0.3, the youngest Galactic SNR that shows a flux density increasing with time (Green et al. 2008), is also shown (triangle), but it is not included in the calibration sample because it is still in the early (rising) free expansion phase of evolution (see Berezhko & Völk 2004).

(low correlation coefficient<sup>12</sup>  $r = -0.68$ ). Much of this dispersion is due to properties of the SN explosion and ISM, which may substantially differ from one SNR to another. It has generally been accepted that the density of the ISM is of significant importance in the evolution of SNRs; the other parameters are, in one way or another, connected to the ISM density (Arbutina & Urošević 2005). SNRs of different types can be found along more or less parallel tracks in the  $\Sigma$ - $D$  plane. Also, the environment is probably quite inhomogeneous in the case of a single SNR, which would add more confusion in statistical studies. The errors of determined distances and, to a lesser extent, flux densities of the calibrator sample both directly affect the scatter in the graph.

Theoretical considerations assume that the  $\Sigma$ - $D$  relation corresponds to the evolutionary track of a typical SNR.

Even for the Sedov phase, the fit should not necessarily be assumed to be linear (in log-log space), and Sedov sub-phases have  $\beta$  slopes from 2 to 5.75 as shown in Section 2. The previously described effects add an extra scatter in our sample of calibrators.

Due to the lack of information, it is not possible to separate all SNRs according to their intrinsic properties, which are connected with the density of the ISM in which they expand their evolutionary stage. We therefore expect to obtain an averaged empirical  $\Sigma$ - $D$  relation that may still be used as a distance estimator in cases when other existing methods are

<sup>11</sup> The sixth regression method, the arithmetic mean of the OLS( $Y|X$ ) and OLS( $X|Y$ ) slopes, was not contained in their paper, but was added in the proof.

<sup>12</sup> Pearson product-moment correlation coefficient is calculated using the following equation:  $r = \frac{\sum_{i=0}^n (x_i - \bar{x})(y_i - \bar{y})}{\sqrt{\sum_{i=0}^n (x_i - \bar{x})^2} \sqrt{\sum_{i=0}^n (y_i - \bar{y})^2}}$ .

inapplicable. Errors of distances obtained by this method will not be negligible but are still acceptable for the above purpose (the average fractional error of the CB98 relation defined as  $f = (d_{\text{obs}} - d_{\text{sd}}/d_{\text{obs}})$  was about 40%).

We perform a set of Monte Carlo simulations to estimate the influence of the scatter of data on the  $\Sigma$ - $D$  slope. We generate random SNR populations (50–5000 SNRs) according to artificially chosen  $\Sigma$ - $D$  relations with  $\beta$  slopes 2, 3, 4, 5, and 6, covering roughly the expected interval of slopes in the Sedov phase. For each randomly selected value of  $D$  from interval 5 to 150 pc (similar to that of real data), we calculate surface brightness  $\Sigma$  using the initially proposed relation. Then we add random “polar” scatter in the created log–log data set. We add scatter by choosing random angle  $\phi$  and random distance  $r$  from original point  $(x, y)$ , after which we perform the following transformation  $(x, y) \mapsto (x + r \cos \phi, y + r \sin \phi)$ . For obtaining random angle  $\phi$  and distance  $r$ , respectively, we use uniform distribution and  $\chi^2$  distribution with 10 degrees of freedom (usually labeled as  $\chi_{10}^2$ ), implemented in the GSL<sup>13</sup> numerical library for C programming language. We have chosen this distance distribution to be close to normal distribution, although additional tests showed that the type of distribution and number of degrees of freedom (for  $\chi^2$ ) does not significantly affect our later conclusions. The only parameter that we enter is the distance that occurs most frequently in a generated distribution of distances (known as the mode in statistics), which is a direct measure of dispersion from generated artificial samples (denoted by  $r_{\text{mode}}$ ). Such a mode value ensures that the artificial distribution is similar to the real distributions for the 60 SNRs sample fitted with six different regression methods ( $r_{\text{mode}} \approx 0.5$ ).

We give values of fitted slopes for randomly generated SNR populations in Figure 2 as a function of sample size and regression method (orthogonal, arithmetic mean, geometric mean, bisector, OLS( $Y|X$ ) and OLS( $X|Y$ ) regression). Each figure also contains information about the value of simulated slope  $\beta$  before performing random scatter on the log–log data set.

After inspection of graphs in Figure 2, we come to the conclusion that orthogonal regression gives  $\beta$  slopes that are closest to the initial slopes of the artificially generated samples. Also, this type of regression shows significant stability as it converges to narrow value intervals for larger sample sizes.

This means that orthogonal regression is least sensitive to the scatter in the  $\Sigma$ - $D$  plane. As mentioned at the beginning of this section, data dispersion is large in the calibration set that is used to construct our new empirical Galactic  $\Sigma$ - $D$  relation. Although Isobe et al. (1990) concluded that the bisector performs significantly better than orthogonal regression, our class of problems (with large intrinsic scatter and steep slopes) gives more reliable solutions when solved with orthogonal regression. The existence of this significant scattering is obvious from the plots. It occurs as a result of the coupling of several intrinsic SNR properties related to energy liberated by SN explosions, the density of surrounding media, and the evolutionary status of the remnants. The results of our Monte Carlo simulations (see Figure 2) show that the orthogonal regression gives fitted slopes that are closest in value to the simulated slopes. Therefore, we strongly suggest orthogonal regression, instead of the previously used OLS( $Y|X$ ) and other regression types, for obtaining any kind of empirical  $\Sigma$ - $D$  relation with slopes between 2 and 6. All

previous Galactic empirical relations have slopes in this interval (see Urošević 2002).

After applying non-weighted orthogonal regression on the sample containing 60 calibrators from Table 1, we obtain the relation

$$\Sigma_{1\text{GHz}} = 3.25_{-2.91}^{+27.94} \times 10^{-14} D^{-4.8 \pm 0.7} \text{ W m}^{-2} \text{ Hz}^{-1} \text{ sr}^{-1}. \quad (18)$$

The new relation is significantly steeper than those obtained in earlier studies. The results of our Monte Carlo simulation (see Figure 2) also give such a steep slope for the examined relation. Moreover, the orthogonal fit gives steeper slopes than any other regression, except OLS( $X|Y$ ). Shell SNRs with distances derived from our  $\Sigma$ - $D$  relation are shown in Table 3. In total, 207 remnants are shown.

Next, we define fractional errors

$$f = \left| \frac{d_1 - d_\Sigma}{d_1} \right| \quad (19)$$

in order to get an estimate of the accuracy of the  $\Sigma$ - $D$  relation for individual SNR distances and also as an indicator of the applicability of our relation for distance determination. Here,  $d_1$  is the independently determined distance to an SNR and  $d_\Sigma$  is the distance derived from the  $\Sigma$ - $D$  relation. The average fractional error is  $\bar{f} = 0.47$  (comparable to that of CB98  $\bar{f} = 0.41$ , although we use a significantly larger sample). We also give average fractional errors for all six regressions in Table 2.

The Monte Carlo simulations presented here show that orthogonal regression is stabler for larger samples (see Figure 2), so our calibration data set (60 SNRs) does not represent a proper sample for obtaining a high accuracy  $\Sigma$ - $D$  relation. A stabler behavior for larger samples is also the case for the other five regressions.

#### 4.2. $L$ - $D$ Relation

For a proper  $\Sigma$ - $D$  analysis, the  $L$ - $D$  correlation should be checked. Using appropriate definitions of flux density and angular diameter, we have the following dependence  $\Sigma_\nu \propto L_\nu D^{-2}$ . However, the  $\Sigma$ - $D$  relation can be written as

$$\Sigma_\nu = AD^{-2+\delta}, \quad (20)$$

which allows for a possible dependence of luminosity on the linear diameter in the form  $L_\nu = CD^\delta$ , where  $C$  is constant. Radio luminosity as a function of the diameter for the calibrators in Table 1 is given in Figure 3, and a very low correlation is evident. As an illustration, orthogonal regression, applied here, gives  $L$ - $D$  a slope of  $\delta \approx -15.3$ . However, this value does not coincide with the value  $\delta = -3$  obtained in Equation (20) for the relation  $\Sigma \propto D^{-5}$ . Also, CB98 did not find any significant correlation between luminosity and linear diameter for shell type alone or for shell + composite-type distance calibrators. Previous studies of the  $\Sigma$ - $D$  relation indicate that  $\delta \approx 0$ , which leads to a radio luminosity that is independent of diameter and to the so-called trivial relation,  $\Sigma \propto D^{-2}$ . If the  $L$ - $D$  correlation does not exist, the trivial  $\Sigma \propto D^{-2}$  form should not be used (Arbutina et al. 2004).

Similar to the previous subsection, we also perform a set of Monte Carlo simulations to estimate the influence of the severe scatter of data on the  $L$ - $D$  slope. We use a randomly generated  $\Sigma$ - $D$  sample with added random polar scatter to construct  $L$ - $D$  scatter by applying the luminosity–surface-brightness relation  $L_\nu = \pi^2 D^2 \Sigma_\nu$ .

<sup>13</sup> GNU Scientific Library (GSL), <http://www.gnu.org/software/gsl/>

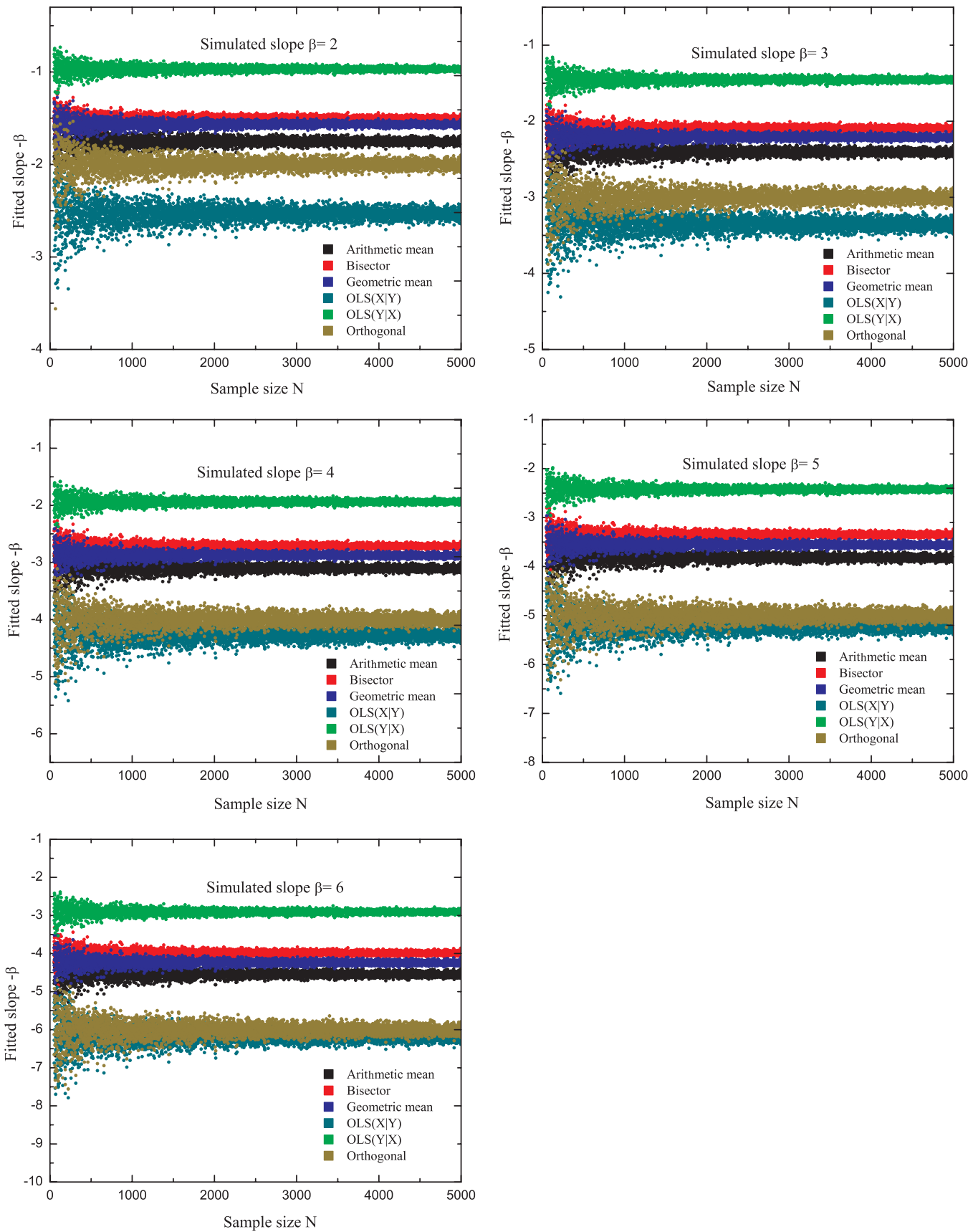


**Figure 2.** Fitted  $\Sigma$ - $D$  slopes vs. sample sizes for six regression types applied on randomly generated SNR samples containing artificial scatter and simulated slopes  $\beta = 2, 3, 4, 5,$  and  $6$ . This analysis was done to determine which type of regression is the least sensitive to scattering. (A color version of this figure is available in the online journal.)

**Table 3**  
Distances to Shell SNRs Calculated from Our  $\Sigma$ - $D$  Relation

Catalog Name	Other Name	Flux density (Jy)	Diameter (pc)	Distance (kpc)
G0.0+0.0	Sgr A East	100.0	8.0	9.3
G0.3+0.0		22.0	18.4	5.8
G1.0-0.1		15.0	17.5	7.5
G1.4-0.1		2.0	28.8	9.9
G1.9+0.3		0.6	17.1	<sup>a</sup>
G3.7-0.2		2.3	30.5	8.5
G3.8+0.3		3.0	33.6	6.4
G4.2-3.5		3.2	39.7	4.9
G4.5+6.8	Kepler, SN1604, 3C358	19.0	11.2	12.9 (6.0) <sup>b</sup>
G4.8+6.2		3.0	33.6	6.4
G5.2-2.6		2.6	34.6	6.6
G5.5+0.3		5.5	26.4	6.8
G5.9+3.1		3.3	34.4	5.9
G6.1+0.5		4.5	28.5	6.7
G6.4+4.0		1.3	49.6	5.5
G6.5-0.4		27.0	21.6	4.1
G7.0-0.1		2.5	32.4	7.4
G7.2+0.2		2.8	28.9	8.3
G7.7-3.7	1814-24	11.0	28.1	4.4
G8.3-0.0		1.2	23.1	17.7
G8.7-5.0		4.4	36.1	4.8
G8.7-0.1	W30	80.0	25.1	1.9
G8.9+0.4		9.0	30.3	4.3
G9.7-0.0		3.7	28.1	7.5
G9.8+0.6		3.9	27.1	7.8
G9.9-0.8		6.7	24.3	7.0
G10.5-0.0		0.9	27.5	15.8
G11.0-0.0		1.3	31.3	10.8
G11.1-1.0		5.8	27.1	6.3
G11.1-0.7		1.0	31.4	12.3
G11.1+0.1		2.3	29.0	9.1
G11.2-0.3		22.0	12.3	10.5 (4.4) <sup>b</sup>
G11.4-0.1		6.0	21.1	9.1
G11.8-0.2		0.7	24.6	21.1
G12.0-0.1		3.5	22.3	10.9
G12.2+0.3		0.8	27.2	17.0
G12.7-0.0		0.8	28.2	16.1
G13.5+0.2		3.5	18.6	14.3
G14.1-0.1		0.5	29.9	18.7
G14.3+0.1		0.6	26.5	20.4
G15.1-1.6		5.5	35.0	4.5
G15.4+0.1		5.6	27.2	6.4
G15.9+0.2		5.0	19.4	11.3
G16.0-0.5		2.7	29.4	8.3
G16.2-2.7		2.0	35.7	7.2
G16.4-0.5		4.6	27.0	7.2
G17.0-0.0		0.5	28.8	19.8
G17.4-2.3		4.8	34.3	4.9
G17.4-0.1		0.4	32.4	18.6
G17.8-2.6		4.0	35.6	5.1
G18.1-0.1		4.6	22.2	9.6
G18.6-0.2		1.4	25.2	14.4
G18.8+0.3	Kes 67	33.0	18.6	4.7 (12.0) <sup>b</sup>
G19.1+0.2		10.0	31.1	4.0
G20.4+0.1		3.1	24.1	10.3
G21.0-0.4		1.1	29.6	12.8
G21.5-0.1		0.4	30.1	20.7
G21.8-0.6	Kes 69	69.0	18.6	3.2 (5.2) <sup>b</sup>
G22.7-0.2		33.0	24.0	3.2
G23.3-0.3	W41	70.0	21.0	2.7 (4.2) <sup>b</sup>
G24.7-0.6		8.0	25.6	5.9
G27.4+0.0	Kes 73, 4C-04.71	6.0	15.9	13.7 (8.65) <sup>b</sup>
G28.6-0.1		3.0	27.4	8.7
G29.6+0.1		1.5	23.1	15.9
G30.7+1.0		6.0	31.0	5.1
G31.5-0.6		2.0	36.5	7.0
G31.9+0.0	3C391	24.0	14.1	8.2 (8.5) <sup>b</sup>
G32.0-4.9	3C396.1	22.0	36.6	2.1

**Table 3**  
(Continued)

Catalog Name	Other Name	Flux density (Jy)	Diameter (pc)	Distance (kpc)
G32.4+0.1		0.2	35.6	20.4
G32.8-0.1	Kes 78	11.0	25.3	5.1
G33.2-0.6		3.5	32.6	6.2
G33.6+0.1	Kes 79, 4C00.70, HC13	22.0	17.7	6.1 (7.0) <sup>b</sup>
G36.6+2.6		0.7	41.7	9.7
G40.5-0.5		11.0	28.1	4.4
G41.1-0.3	3C397	22.0	11.4	11.7 (10.3) <sup>b</sup>
G42.8+0.6		3.0	37.8	5.4
G43.3-0.2	W49B	38.0	10.4	10.3 (10.0) <sup>b</sup>
G43.9+1.6		8.6	44.2	2.5
G45.7-0.4		4.2	34.1	5.3
G46.8-0.3	HC30	14.0	22.8	5.3 (7.8) <sup>b</sup>
G49.2-0.7	W51	160.0	18.5	2.1
G53.6-2.2	3C400.2, NRAO 611	8.0	34.1	3.9 (2.8) <sup>b</sup>
G54.4-0.3	HC40	28.0	29.6	2.5 (3.3) <sup>b</sup>
G55.0+0.3		0.5	47.5	9.4 (14.0) <sup>b</sup>
G55.7+3.4		1.4	43.3	6.5
G57.2+0.8	4C21.53	1.8	31.6	9.1
G59.5+0.1		3.0	31.2	7.2
G65.1+0.6		5.5	50.6	2.6 (9.0) <sup>b</sup>
G65.3+5.7		52.0	56.6	0.7
G67.7+1.8		1.0	37.3	9.5
G69.7+1.0		2.0	33.9	7.8
G73.9+0.9		9.0	31.7	4.0
G74.0-8.5	Cygnus Loop	210.0	37.1	0.7 (0.54) <sup>b</sup>
G78.2+2.1	DR4, gamma Cygni SNR	320.0	21.3	1.2 (1.2) <sup>b</sup>
G82.2+5.3	W63	120.0	29.0	1.3
G83.0-0.3		1.0	30.2	13.1
G84.2-0.8		11.0	25.8	5.0 (4.5) <sup>b</sup>
G89.0+4.7	HB21	220.0	28.7	0.9 (0.8) <sup>b</sup>
G93.3+6.9	DA 530, 4C(T)55.38.1	9.0	30.3	4.5 (2.2) <sup>b</sup>
G93.7-0.2	CTB 104A, DA 551	65.0	33.0	1.4 (1.5) <sup>b</sup>
G94.0+1.0	3C434.1	13.0	29.6	3.7 (5.2) <sup>b</sup>
G96.0+2.0		0.3	62.0	8.2 (4.0) <sup>b</sup>
G108.2-0.6		8.0	45.3	2.5 (3.2) <sup>b</sup>
G109.1-1.0	CTB 109	22.0	26.9	3.3 (3.2) <sup>b</sup>
G111.7-2.1	Cassiopeia A, 3C461	2720.0	5.1	3.5 (3.4) <sup>b</sup>
G114.3+0.3		5.5	51.6	2.5 (0.7) <sup>b</sup>
G116.5+1.1		10.0	45.4	2.3 (1.6) <sup>b</sup>
G116.9+0.2	CTB 1	8.0	35.7	3.6 (1.6) <sup>b</sup>
G119.5+10.2	CTA 1	36.0	39.0	1.5 (1.4) <sup>b</sup>
G120.1+1.4	Tycho, 3C10, SN1572	56.0	13.4	5.8 (4.0) <sup>b</sup>
G126.2+1.6		6.0	50.6	2.5
G127.1+0.5	R5	12.0	36.8	2.8 (1.25) <sup>b</sup>
G132.7+1.3	HB3	45.0	35.5	1.5 (2.2) <sup>b</sup>
G156.2+5.7		5.0	62.9	2.0 (1.0) <sup>b</sup>
G160.9+2.6	HB9	110.0	36.1	1.0 (0.8) <sup>b</sup>
G166.0+4.3	VRO 42.05.01	7.0	40.6	3.2 (4.5) <sup>b</sup>
G179.0+2.6		7.0	49.0	2.4
G180.0-1.7	S147	65.0	45.8	0.9 (0.62) <sup>b</sup>
G182.4+4.3		1.2	61.1	4.2
G189.1+3.0	IC443, 3C157	160.0	21.8	1.7 (1.5) <sup>b</sup>
G192.8-1.1	PKS 0607+17	20.0	41.4	1.8
G205.5+0.5	Monoceros Nebula	160.0	41.4	0.6 (1.2) <sup>b</sup>
G206.9+2.3	PKS 0646+06	6.0	43.8	3.1
G260.4-3.4	Puppis A, MSH 08-44	130.0	24.6	1.5 (2.2) <sup>b</sup>
G261.9+5.5		10.0	34.3	3.4
G266.2-1.2	RX J0852.0-4622	50.0	41.0	1.2
G272.2-3.2		0.4	46.9	10.7
G279.0+1.1		30.0	41.3	1.5
G284.3-1.8	MSH 10-53	11.0	29.1	4.2
G286.5-1.2		1.4	33.8	9.3
G289.7-0.3		6.2	27.6	6.0
G290.1-0.8	MSH 11-61A	42.0	19.0	4.0 (7.0) <sup>b</sup>
G292.2-0.5		7.0	27.9	5.5 (8.4) <sup>b</sup>
G296.1-0.5		8.0	34.1	3.9
G296.5+10.0	PKS 1209-51/52	48.0	34.4	1.5 (2.1) <sup>b</sup>
G296.8-0.3	1156-62	9.0	26.2	5.4 (9.6) <sup>b</sup>

**Table 3**  
(Continued)

Catalog Name	Other Name	Flux density (Jy)	Diameter (pc)	Distance (kpc)
G298.6−0.0		5.0	24.3	8.0
G299.2−2.9		0.5	43.7	10.7
G299.6−0.5		1.0	36.8	9.7
G301.4−1.0		2.1	43.9	5.2
G302.3+0.7		5.0	29.6	6.0
G304.6+0.1	Kes 17	14.0	17.8	7.6
G308.1−0.7		1.2	35.5	9.4
G309.2−0.6		7.0	25.2	6.4
G309.8+0.0		17.0	25.6	4.0 (3.6) <sup>b</sup>
G310.6−0.3	Kes 20B	5.0	21.9	9.4
G310.8−0.4	Kes 20A	6.0	24.8	7.1
G311.5−0.3		3.0	20.1	13.8
G312.4−0.4		45.0	26.3	2.4
G312.5−3.0		3.5	33.3	6.0
G315.4−2.3	RCW 86, MSH 14−63	49.0	26.9	2.2 (2.3) <sup>b</sup>
G315.9−0.0		0.8	44.6	8.2
G316.3−0.0	MSH 14−57	20.0	24.0	4.1
G317.3−0.2		4.7	25.2	7.9
G321.9−0.3		13.0	29.3	3.8
G323.5+0.1		3.0	29.5	7.8
G327.2−0.1		0.4	30.1	20.7
G327.4+0.4	Kes 27	30.0	22.5	3.7 (4.85) <sup>b</sup>
G327.4+1.0		1.9	33.3	8.2
G327.6+14.6	SN1006, PKS 1459−41	19.0	28.5	3.3 (2.2) <sup>b</sup>
G330.0+15.0	Lupus Loop	350.0	32.6	0.6
G330.2+1.0		5.0	24.9	7.8
G332.0+0.2		8.0	23.4	6.7
G332.4−0.4	RCW 103	28.0	16.9	5.8 (3.1) <sup>b</sup>
G332.4+0.1	MSH 16−51, Kes 32	26.0	20.2	4.6
G332.5−5.6		2.0	47.7	4.7
G335.2+0.1		16.0	25.5	4.2
G336.7+0.5		6.0	24.7	7.2
G337.0−0.1	CTB 33	1.5	14.2	32.5 (11.0) <sup>b</sup>
G337.2−0.7		1.5	24.8	14.2
G337.3+1.0	Kes 40	16.0	21.3	5.5
G337.8−0.1	Kes 41	18.0	16.3	7.6 (11.0) <sup>b</sup>
G338.1+0.4		4.0	29.5	6.8
G338.3−0.0		7.0	20.4	8.8 (11.0) <sup>b</sup>
G338.5+0.1		12.0	19.2	7.3
G340.4+0.4		5.0	22.3	9.1
G340.6+0.3		5.0	19.5	11.2 (15.0) <sup>b</sup>
G341.9−0.3		2.5	23.8	11.7
G342.0−0.2		3.5	26.1	8.6
G342.1+0.9		0.5	37.3	13.5
G343.1−0.7		7.8	31.0	4.5
G344.7−0.1		2.5	27.5	9.5 (6.3) <sup>b</sup>
G345.7−0.2		0.6	29.9	17.1
G346.6−0.2		8.0	19.9	8.5 (11.0) <sup>b</sup>
G348.5−0.0		10.0	20.8	7.2
G348.5+0.1	CTB 37A	72.0	16.5	3.8 (7.9) <sup>b</sup>
G348.7+0.3	CTB 37B	26.0	21.3	4.3 (13.2) <sup>b</sup>
G349.2−0.1		1.4	27.3	12.8
G349.7+0.2		20.0	9.9	15.2 (18.4) <sup>b</sup>
G350.0−2.0		26.0	31.5	2.4
G351.7+0.8		10.0	25.1	5.4
G351.9−0.9		1.8	29.9	9.9
G352.7−0.1		4.0	21.6	10.7 (7.5) <sup>b</sup>
G353.6−0.7		2.5	42.9	4.9
G353.9−2.0		1.0	36.8	9.7
G354.8−0.8		2.8	34.8	6.3
G355.4+0.7		5.0	34.6	4.8
G355.6−0.0		3.0	22.9	11.3
G355.9−2.5		8.0	24.2	6.4
G356.2+4.5		4.0	36.2	5.0
G356.3−0.3		3.0	25.2	9.9
G356.3−1.5		3.0	33.1	6.6
G357.7+0.3		10.0	29.6	4.2
G358.0+3.8		1.5	52.3	4.7

**Table 3**  
(Continued)

Catalog Name	Other Name	Flux density (Jy)	Diameter (pc)	Distance (kpc)
G358.1+0.1		2.0	38.1	6.5
G358.5−0.9		4.0	31.0	6.3
G359.0−0.9		23.0	24.6	3.7
G359.1−0.5		14.0	27.7	4.0 (7.6) <sup>b</sup>

**Notes.**

<sup>a</sup> Using our  $\Sigma$ - $D$  relation for this SNR makes no sense since it is reliably established that G1.9+0.3 is increasing in its flux density.

<sup>b</sup> SNRs belonging to our new calibration sample from Table 1. Values in brackets represent directly obtained distances.

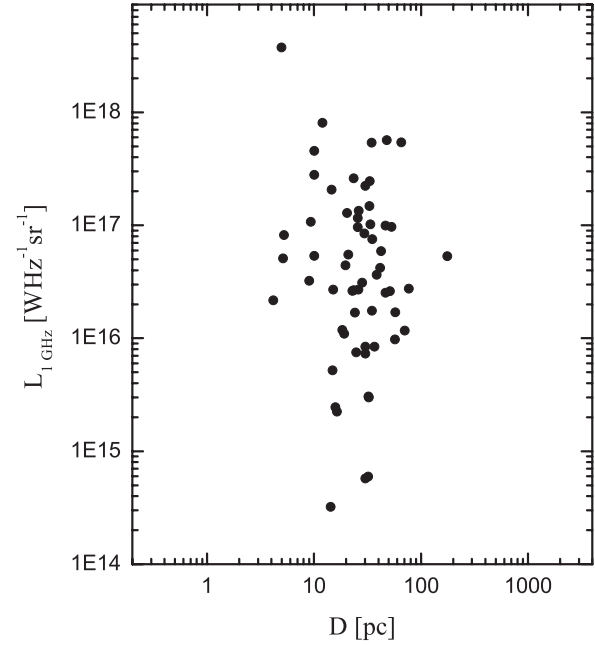


**Figure 3.** Radio luminosity (at 1 GHz) vs. the diameter for the SNRs( $\Sigma$ - $D$  calibrators) given in Table 1, to allow a possible dependence of the luminosity on linear diameter in the form of  $L_v = CD^\delta$ . Weak correlation is evident, primarily due to severe data scatter.

Six regression methods were applied on randomly generated  $L$ - $D$  samples. Figure 4 shows fitted  $L$ - $D$  slopes  $\delta$  as a function of sample size, with a scatter  $r_{\text{mode}} = 0.5$  and the simulated  $\Sigma$ - $D$  slope  $\beta = 5$ . At first glance, Figure 4 leads to the conclusion that OLS( $Y|X$ ), bisector, and geometric mean regression (average  $\delta$  values of  $-0.42$ ,  $-1.41$ , and  $-2.64$ , respectively) give much flatter slopes than arithmetic mean, orthogonal, and OLS( $X|Y$ ) regressions ( $\delta$   $-8.84$ ,  $-14.90$ , and  $-17.25$ , respectively). We note that orthogonal regression, which is of significant importance for us, gives a very similar slope ( $-14.9$ ) for randomly scattered data as that for real data ( $-15.3$ ), which is very good agreement but of no physical importance. The orthogonal fit performs very unstably, especially for lower sample sizes ( $N < 500$ ) and it is strongly influenced by data scatter, as are the other five fitting methods. Although OLS( $Y|X$ ), bisector, and geometric mean regression seem more stable than the other three methods, converting their slopes into an angle interval leads to the opposite conclusion.

The main reason for this instability can be inferred from a brief inspection of Figure 5. When we increase the scatter of the simulated data sets, the distribution of points tends to be almost vertical and even severe scatter can change the fitted

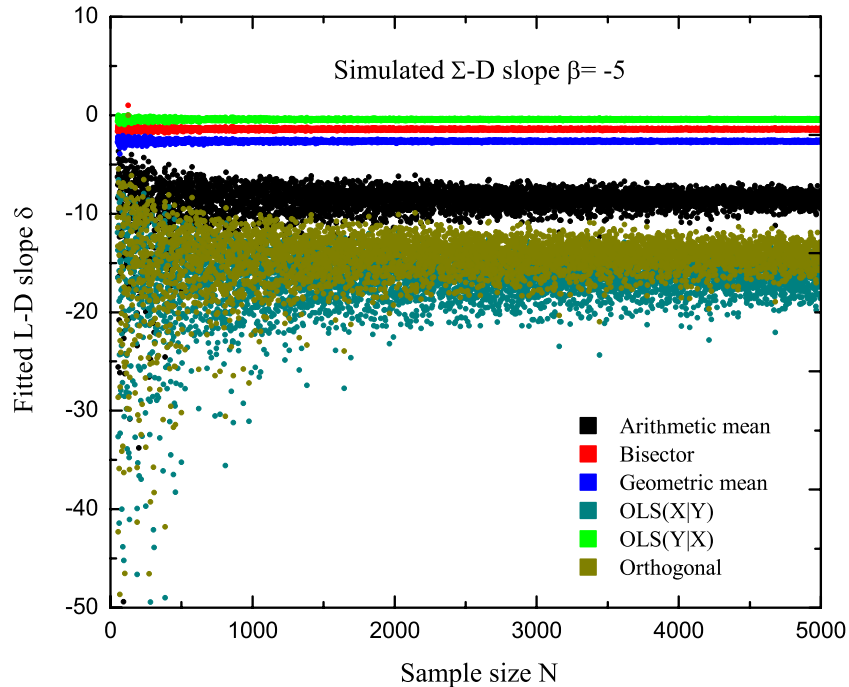


**Figure 4.** Fitted slopes of the power-law fit  $L_v = CD^\delta$  vs. sample sizes for six regression types applied on randomly generated samples ( $r_{\text{mode}} = 0.5$ ). It is evident that the orthogonal fit becomes very unstable for the  $L$ – $D$  relation and strongly influenced by data scatter, especially for a small number of points, as is the case with our sample.

(A color version of this figure is available in the online journal.)

slope from negative to positive. This effect produces a break in the dependence of the orthogonal fit slope from data dispersion ( $r_{\text{mode}}$ ). This may be due to a lower span of luminosities for the  $L$ – $D$  relation in comparison to the span of surface brightness for  $\Sigma$ – $D$  relation (spans of diameters are the same for both relations).

It can be inferred from further analysis that, taking into account all six fitting procedures, the geometric mean regression gives a slope that is close to that expected,  $\delta = -\beta + 2$  (for simulated  $\Sigma$ – $D$  slope  $\beta = 6, 5, 4, 3$ ). Figure 6 also shows that the geometric mean regression can be a valid tool for obtaining  $L$ – $D$  relation for a limited range of data dispersion. Thus, we should be careful if geometric mean regression is applied on  $L$ – $D$  analysis since it is not insensitive to severe scatter, such as orthogonal regression, when applied on  $\Sigma$ – $D$  relation.

Therefore, we suggest obtaining the  $L$ – $D$  relation directly by using some type of regression only if the data set of calibrators is not subject to severe scatter. In other cases, a more accurate approach would first require the derivation of the  $\Sigma$ – $D$  relation from which then, by using Equation (20), we obtain the  $L$ – $D$  relation. Our conclusion is also supported by the fact that Arbutina et al. (2004) did not find any significant correlation when analyzing  $L$ – $D$  dependence, except for the M82 starburst galaxy (with a fit quality of 64%), for which a good  $\Sigma$ – $D$  relation does exist.

## 5. DISTANCES OF TWO NEWLY FOUND GALACTIC SNRS: G25.1–2.3 AND G178.2–4.2

The Sino-German  $\lambda 6$  cm Galactic plane survey is a sensitive survey with the potential to detect new low-surface-brightness SNRs. This survey searches for new shell-like objects in the  $\lambda 6$  cm survey maps and studies their radio emission,

polarization, and spectra using the  $\lambda 6$  cm maps together with the  $\lambda 11$  cm and  $\lambda 21$  cm Effelsberg observations.

Gao et al. (2011) have discovered two new large faint SNRs, G25.1–2.3 and G178.2–4.2, both of which show shell structure. G25.1–2.3 is revealed by its strong southern shell, which has a size of  $80' \times 30'$ . It has a non-thermal radio spectrum with a spectral index of  $\alpha = -0.49 \pm 0.13$ . G178.2–4.2 has a size of  $72' \times 62'$  with strongly polarized emission being detected along its northern shell. The spectrum of G178.2–4.2 is also non-thermal, with an integrated spectral index of  $\alpha = -0.48 \pm 0.13$ . Its low surface brightness makes G178.2–4.2 the second faintest known Galactic SNR. This demonstrates that more large and faint SNRs exist, but are very difficult to detect.

Using the total intensity and the radio spectral index, Gao et al. (2011) calculated the surface brightness of both objects at 1 GHz, obtaining  $\Sigma_{1\text{GHz}} = 5.0 \times 10^{-22} \text{ W m}^{-2} \text{ Hz}^{-1} \text{ sr}^{-1}$  for the southern shell of G25.1–2.3 and  $\Sigma_{1\text{GHz}} = 7.2 \times 10^{-23} \text{ W m}^{-2} \text{ Hz}^{-1} \text{ sr}^{-1}$  for G178.2–4.2.

The  $\Sigma$ – $D$  relation of CB98 was used to estimate the distances of the two newly found SNRs. For G25.1–2.3, they found that the diameter for the shell is 72 pc and the distance was 3.1 kpc, consistent with those derived from the H I data. For G178.2–4.2, they found that the diameter is 197 pc and its distance is 9.4 kpc. This places the object far outside the Galaxy, which seems hardly possible, as the authors have pointed out in their paper.

This is the appropriate place to mention specific behavior of the  $\Sigma$ – $D$  relation, depending on the brightness of the SNR for which the distance is calculated. The slope of the  $\Sigma$ – $D$  relation directly affects derived diameters and hence distances. A steeper slope will give larger diameters (and hence distances) for SNRs with higher surface brightnesses, while it will lead to smaller diameters (distances) for SNRs with lower surface brightnesses.

We applied our new Galactic  $\Sigma$ – $D$  relation to obtain the distances of these two objects. For G25.1–2.3, we find that

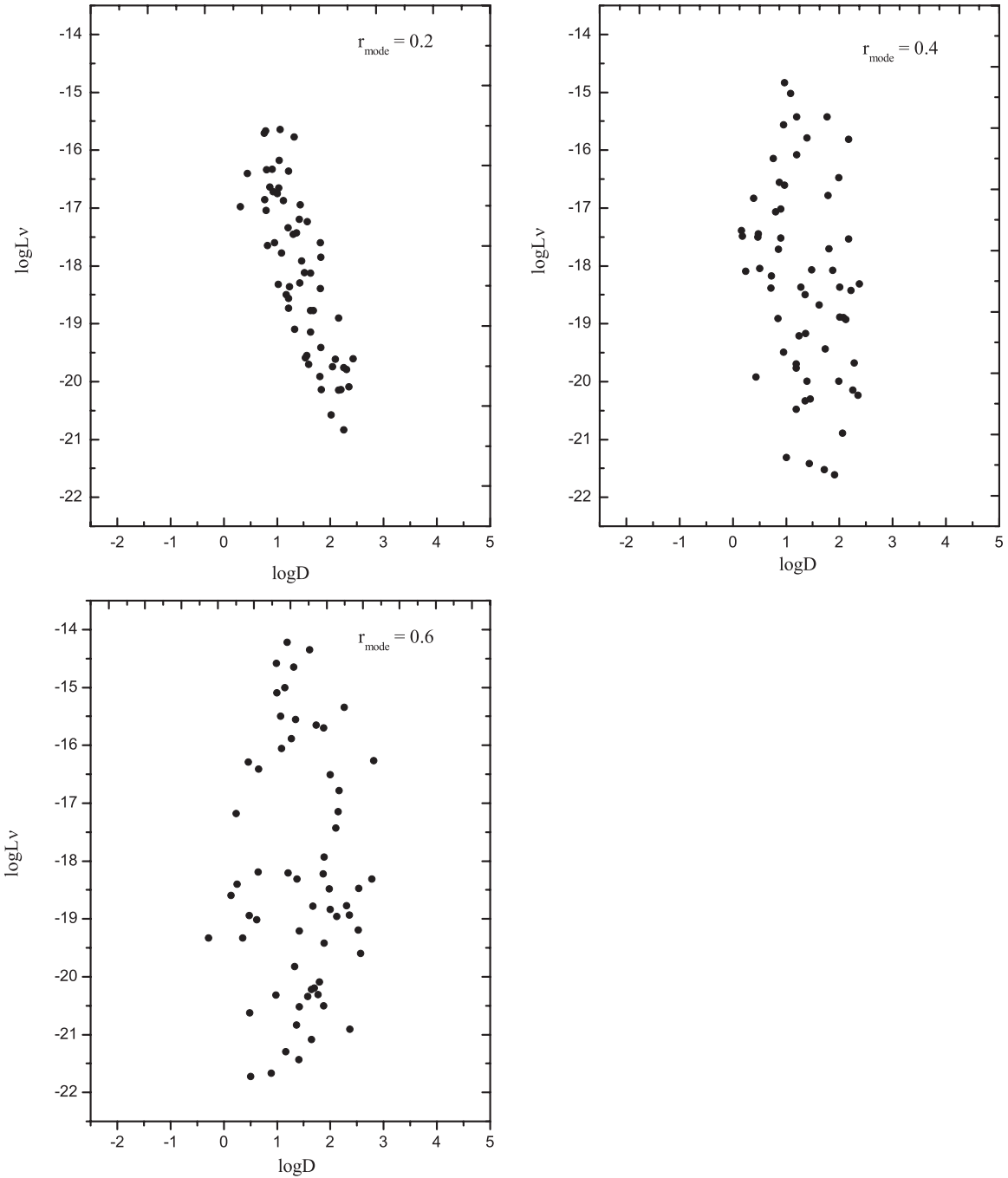


**Figure 5.** Appearance of the  $L$ – $D$  relation with increasing data dispersion (quantified with parameter  $r_{\text{mode}}$ ). It can be inferred from the plots that larger scattering leads to the decrease and even loss of the correlation.

the diameter for the shell is 42 pc and hence the distance is 1.8 kpc, which is still not far from that derived from the H I data. For G178.2–4.2, we find that the corresponding diameter is only 63 pc, so its distance is 3.0 kpc, which places the object inside the Milky Way. Note, however, that the uncertainties of these estimates could be as large as 50%.

## 6. DEPENDENCE OF $\Sigma$ – $D$ RELATION ON THE DENSITY OF THE INTERSTELLAR MEDIUM

We focus on a more direct connection between the ISM density and the  $\Sigma$ – $D$  relation. Duric & Seaquist (1986) assumed that the dependence of surface brightness on the density of the

ISM has the form  $\Sigma \propto \rho_0^\eta \propto n_{\text{H}}^\eta$ , where  $\rho_0$  and  $n_{\text{H}}$  are the average ambient density and hydrogen number density, respectively, and  $\eta$  is a constant (see also Berezhko & Völk 2004). This means, the larger the surrounding ISM density, the greater the synchrotron emission from the SNR.

This suggests that, on average, SNRs in dense environments would tend to have higher surface brightness in comparison to those evolving in lower-density media. However, since the  $\Sigma = AD^{-17/4}$  relation depends primarily on the initial explosion energy (Equation (16)), variation in SN energy rather than density could produce scattering in some parts of the  $\Sigma$ – $D$  diagram.

Although it is difficult to decide which SNRs should be included or excluded from analysis, we tried to extract subsamples

**Table 4**  
Basic Properties of the 28 Galactic SNRs Evolving in Dense ISM, i.e., Associated with Molecular Clouds

Catalog Name	Conventional Name	Evidence	Surface Brightness ( $\text{W m}^{-2} \text{Hz}^{-1} \text{sr}^{-1}$ )	Diameter (pc)
G18.8+0.3 <sup>a</sup>	Kes 67	CO MA & LB, CO ratio	2.66e-20	47.7
G21.8-0.6	Kes 69	OH, CO MA & LB, HCO+, H <sub>2</sub>	2.60e-20	30.3
G23.3-0.3	W41	H I MA & CO RC, extended TeV	1.45e-20	33.0
G31.9+0.0 <sup>a</sup>	3C391	OH, molecular MA & LB (CO, HCO+, CS), H <sub>2</sub> , NIR	1.03e-19	14.6
G33.6+0.1 <sup>a</sup>	Kes 79	CO MA, HCO+ MA, broad OH absorption	3.31e-20	20.4
G41.1-0.3	3C397	CO MA & LB	2.94e-19	10.0
G43.3-0.2 <sup>a</sup>	W49B	H <sub>2</sub> MA, CO ratio	4.77e-19	10.1
G54.4-0.3 <sup>a</sup>	HC40	CO MA & LB, IR MA	2.63e-21	38.4
G78.2+2.1 <sup>a</sup>	$\gamma$ Cygni, DR4	CO MA	1.34e-20	20.9
G84.2-0.8 <sup>a</sup>		CO MA	5.17e-21	23.4
G89.0+4.7 <sup>a</sup>	HB21	CO MA & LB, CO ratio, H <sub>2</sub> , NIR	3.07e-21	24.2
G94.0+1.0	3C434.1	CO RC	2.61e-21	41.4
G109.1-1.0	CTB 109	CO MA & LB	4.22e-21	26.1
G111.7-2.1 <sup>a</sup>	Cassiopeia A, 3C461	H <sub>2</sub> CO absorption, IR RC, CO RC	1.64e-17	4.9
G132.7+1.3 <sup>a</sup>	HB3	CO MA	1.06e-21	51.2
G166.0+4.3 <sup>a</sup>	VRO 42.05.01	unusual shape, CO RC	5.47e-22	57.4
G189.1+3.0	IC443, 3C157	OH, CO ratio, H <sub>2</sub> , molecular MA & LB	1.22E-20	19.6
G205.5+0.5 <sup>a</sup>	Monoceros Nebula	CO RC	4.98e-22	76.8
G260.4-3.4 <sup>a</sup>	Puppis A, MSH 08-44	CO RC, OH(negative)	6.52e-21	35.1
G290.1-0.8	MSH 11-61A	CO RC	2.38e-20	33.2
G332.4-0.4 <sup>a</sup>	RCW 103	IR MA & colors, NIR, H <sub>2</sub> & HCO+ MA	4.21e-20	9.0
G337.0-0.1	CTB 33	OH	1.34e-19	4.2
G337.8-0.1	Kes 41	OH	5.02e-20	23.5
G344.7-0.1		IR RC & colors	3.76e-21	18.3
G346.6-0.2		OH, H <sub>2</sub> , IR colors	1.88E-20	25.6
G348.5+0.1 <sup>a</sup>	CTB 37A	OH, H <sub>2</sub> , IR MA	4.82e-20	34.5
G349.7+0.2 <sup>a</sup>		OH, CO MA & LB, CO ratio, H <sub>2</sub> , IR MA	6.02e-19	12.0
G359.1-0.5 <sup>a</sup>		OH, CO & H <sub>2</sub> MA, HCO+ & CS absorption	3.66e-21	53.1

**Notes.** Evidence: chief evidence that suggests the interaction between SNR and molecular clouds. LB = line broadening, MA = morphology agreement, H<sub>2</sub> = vibrational/rotational lines of molecular hydrogen [e.g., H<sub>2</sub> 1-0 S(1) line (2.12  $\mu\text{m}$ ), H<sub>2</sub> 0-0 S(0)-S(7) lines], NIR = Near-infrared (e.g., [Fe II] line), OH = 1720 MHz OH maser, RC = rough morphological correspondence, etc. (taken from the List of Galactic SNRs Interacting with Molecular Clouds by Jiang et al. 2010).

<sup>a</sup> SNRs belonging to Case & Bhattacharya's (1998) calibration sample.

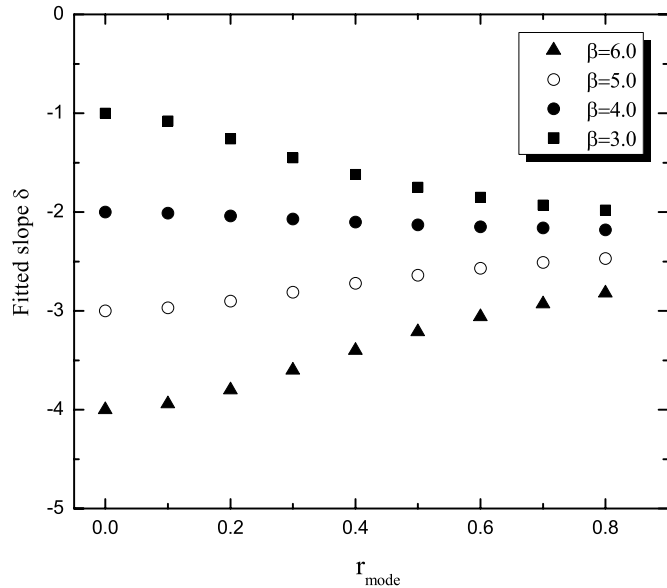


**Figure 6.** Performance of geometric mean regression for fitting power-law  $L-D$  relation  $L_D = CD^\delta$ . This type of regression can be a valid tool for obtaining the  $L-D$  relation only for a limited range of data dispersion and is closest to theoretical value  $\delta = -\beta + 2$ .

of Galactic SNRs (using Table 1) based on the density of the medium in which they evolve and then to obtain particular  $\Sigma-D$  relation.

Mathewson et al. (1983) classified SNRs into four categories based on their optical characteristics: Balmer-dominated, oxygen-rich, plerion/composite, and evolved SNRs. Balmer-dominated line emission is produced when the expanding SNR encounters a low-density ( $\sim 0.1-1 \text{ cm}^{-3}$ ), partially neutral ISM. The hydrogen overrun by the shock is collisionally excited in a thin ( $\lesssim 10^{15} \text{ cm}$ ) ionization zone, producing optical spectra dominated by the Balmer lines of hydrogen (Ghavamian et al. 2007). Oxygen-rich SNRs were mainly identified based on their optical oxygen line emission properties and they primarily occur in H II and molecular cloud regions, i.e., in higher-density regions. Young oxygen-rich SNRs are likely to interact with an especially complex circumstellar medium, rather than the ISM. Balmer-dominated SNRs are connected to Type Ia SNe—deflagration of C/O white dwarf, while oxygen-rich SNRs originate in the Type Ib events—explosions of a massive O or a Wolf-Rayet star.

We created a subsample of 28 Galactic SNRs with known distances, using an online database<sup>14</sup> from Gilles & Samar (2012), interacting with molecular clouds, i.e., evolving in dense ISM. The properties of these SNRs are given in Table 4. After applying orthogonal regression on the subsample from Table 4, the  $\Sigma-D$  relation obtained is

$$\Sigma_{1\text{GHz}} = 3.89_{-2.98}^{+12.81} \times 10^{-15} D^{-3.9 \pm 0.4} \text{ W m}^{-2} \text{ Hz}^{-1} \text{ sr}^{-1}, \quad (21)$$

<sup>14</sup> This work also builds on the List of Galactic SNRs Interacting with Molecular Clouds maintained by Jiang et al., <http://astronomy.nyu.edu.cn/~bjjiang/SNR6.htm>

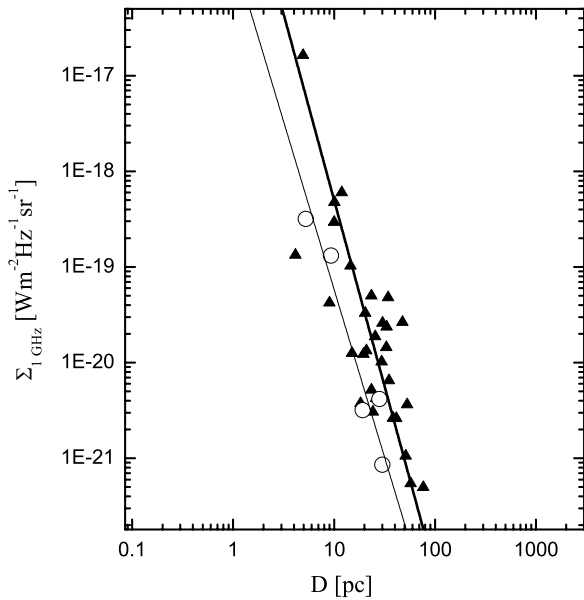


**Figure 7.**  $\Sigma$ - $D$  plots at 1 GHz for Balmer-dominated (empty circles) and oxygen rich SNRs (triangles). The thin line represents the former sample and the thick line represents the later sample. The fit lines are obtained by orthogonal offsets. As expected, remnants evolving in a dense environment lie above those evolving in a low-density medium due to higher synchrotron emission.

which is slightly steeper than the relation  $\beta = 3.5 \pm 0.5$  obtained by Arbutina et al. (2004), whose sample contained only 14 Galactic SNRs associated with molecular clouds. The average fractional error is  $\bar{f} = 0.35$ . Slope  $\beta = 3.9$  for Galactic SNRs in dense ISM is in very good agreement with slope obtained for the M82 data sample by Urošević et al. (2010), who also used orthogonal fitting. Our obtained slope approximately coincides with the conclusion of Berezhko & Völk (2004) that SNRs in dense ISM should populate the part of the line  $\Sigma = AD^{-17/4}$ .

The sample of Galactic SNRs evolving in low-density ISM is significantly smaller. Until now, only five Galactic SNRs showing Balmer-dominated characteristics have been reported (see review papers Vink 2012; Heng 2010) and are therefore thought to expand in low-density medium. The Balmer-dominated subsample contains: Kepler (G4.5+6.8), Cygnus Loop (G74.0–8.5), Tycho (G120.1+1.4), RCW 86 (G315.4–2.3), and SN 1006 (G327.6+14.6), whose basic properties can be found in Table 1. The  $\Sigma$ - $D$  relation obtained is

$$\Sigma_{1\text{GHz}} = 1.89_{-1.29}^{+4.08} \times 10^{-16} D^{-3.5 \pm 0.5} \text{ W m}^{-2} \text{ Hz}^{-1} \text{ sr}^{-1}, \quad (22)$$

with an average fractional error  $\bar{f} = 0.18$ . Figure 7 shows the relation for Balmer-dominated and oxygen-rich Galactic SNRs for comparison purposes. The two relations have similar slopes, but the former is below the latter, as we would expect for SNRs in low-density environments. To further investigate the influence of the ISM density on the  $\Sigma$ - $D$  relation, we should use more complete samples, especially samples of Balmer-dominated remnants.

## 7. SELECTION EFFECTS

Identification of Galactic SNRs is always accompanied by selection effects arising from the difficulty in identifying (1) faint SNRs and (2) small angular size SNRs (e.g., CB98; Green 1991, 2005; Urošević et al. 2005, 2010). A high enough surface brightness for SNRs is required in order to distinguish

them from the background Galactic emission. Any Galactic radio survey is severely biased by observational constraints. The surface-brightness limit seriously affects the completeness of all catalogs of Galactic SNRs and the derived flux densities of many SNRs are also poorly determined. Additionally, small angular size SNRs are likely to be missing from current catalogs and calibration samples. Their small size may cause incorrect classification of SNR type and also lead to incorrect calculation of their surface brightness.

Additionally, Malmquist bias is severe in the Galactic samples, making them incomplete. This is a type of volume selection effect that naturally favors bright objects in any flux-limited survey because they are sampled from a larger spatial volume. The result is a bias against low surface-brightness remnants such as highly evolved old SNRs. Only the extragalactic samples are not influenced by the Malmquist bias since all SNRs in the sample are at essentially the same distance.

Urošević et al. (2010) performed a set of Monte Carlo simulations to estimate the influence of the survey sensitivity selection effect on the  $\Sigma$ - $D$  slope for the M82 sample (31 SNRs). An appropriate sensitivity cutoff is applied to the simulated data points, taking into account only points above the given sensitivity line. They concluded that the sensitivity selection effect does not have a major impact on the  $\Sigma$ - $D$  slope.

Technological advances in radio telescopes and X-ray instruments will greatly increase the number of known SNRs, lead to a better determination of their properties, and thus reduce the influence of the mentioned selection effects.

## 8. SUMMARY AND CONCLUSION

This paper presents a re-analysis of the theoretical and especially empirical Galactic  $\Sigma$ - $D$  relation and the dependence of this relation on the density of the ISM. We were motivated by the observed property that the empirical  $\Sigma$ - $D$  relation strongly depends on the used regression due to severe scatter in data samples. In contrast to the standard least-squares (vertical) regression, we examine the behavior of six different types of regression. We put emphasis on those that satisfy the requirement that the values of parameters obtained from the fitting of  $\Sigma$ - $D$  and  $D$ - $\Sigma$  relations should be invariant within estimated uncertainties, i.e., treat  $\Sigma$  and  $D$  symmetrically (namely: orthogonal regression, bisector, arithmetic, and geometric mean regressions).

The catalog of known Galactic SNRs has grown significantly in size since the work of CB98, from 215 to 274 SNRs. The number of SNRs with known distances has also increased. We included the latest distance updates, if available, to derive a new Galactic  $\Sigma$ - $D$  relation, using a sample of 60 shell SNRs. We concluded from our tests that the size of the sample significantly influences the stability of any type of regression and that more observations are necessary to increase the statistical significance of the sample.

We present an additional modification to the theoretical  $\Sigma$ - $D$  relation for SNRs in the adiabatic expansion (Sedov) phase. This modification is based on the equipartition introduced by Reynolds & Chevalier (1981). Our modification induces a new sub-phase lying between late free expansion and early Sedov phase with a slope of  $\beta = 5.75$ . Our theoretical slope ( $\beta = 4.25$ ) for relatively older SNRs in the Sedov phase is also in agreement with that of Berezhko & Völk (2004).

We have performed an extensive series of Monte Carlo simulations to evaluate numerically how well each of the six regression methods approximate the artificially proposed  $\Sigma$ - $D$

dependence with added scatter. The orthogonal regression is the most accurate slope predictor in data sets with severe scatter, as it gives the slope closest to the original value. For other regression procedures, the fitted slopes of the  $\Sigma$ - $D$  relation are seriously affected by data scatter. Standard (vertical) fitting, or OLS( $Y|X$ ), which was used in previous papers considering empirical  $\Sigma$ - $D$  relation, leads to a significant change in slope when applied on highly dispersed data sets. When the scatter increases, the standard fitting leads to flatter, almost trivial, slopes ( $\beta \approx 2$ ). Also, similar conclusions apply to OLS( $X|Y$ ), bisector, arithmetic, and geometric mean regressions. A possible reason may be the inherent property of  $\Sigma$ - $D$  data sets, which are defined by a narrow range of diameters (about one order of magnitude), in comparison to the wide range of surface brightness (approximately five orders of magnitude). We recommend using orthogonal regression for obtaining any type of empirical  $\Sigma$ - $D$  relation.

Our obtained slope ( $\beta = 4.8$ ) is significantly steeper than previous values, it is far from the trivial one ( $\beta \approx 2.0$ ), and it agrees with theoretical predictions for the Sedov phase of SNR evolution. Since our calibration sample contains 60 SNRs, which probably have different explosion energies, evolve in different ambient density, and may be in different phases of SNR evolution, the relation  $\Sigma \propto D^{-4.8}$  could represent an averaged evolutionary track for Galactic SNRs. As such, it potentially could be used for estimating the distances of SNRs in our Galaxy. A relatively large data scatter can be partly explained by the above mentioned influences.

Additional analysis is carried out to examine the possible dependence of radio luminosity on the linear diameter ( $L$ - $D$  relation) for SNRs. Also, this analysis may provide an answer as to whether determination of SNR distances on the basis of a  $\Sigma$ - $D$  relation is possible. We did not find any significant correlation for our sample consisting of 60 SNRs, while orthogonal regression gives a very steep slope ( $\beta \approx -15$ ) that has no physical meaning. Monte Carlo simulations have revealed that the  $L$ - $D$  relation is very sensitive to severe scatter in the data, which is surely present in our sample. Therefore, it is possible to obtain the  $L$ - $D$  relation only if the set of calibrators is not subject to severe scatter. Otherwise, we obtain very steep slopes without physical meaning. We recommend an indirect approach to obtaining an  $L$ - $D$  relation, which requires obtaining the  $\Sigma$ - $D$  relation first (by orthogonal regression).

We made an attempt to find a homogeneous subsample of Galactic SNRs in low-density and dense environments and to obtain the  $\Sigma$ - $D$  relations for two particular classes of SNRs. Applying orthogonal regression to the sample (which contains 28 SNRs) made of SNRs that evolve in a dense environment of molecular clouds (including oxygen-rich SNRs) leads to the slope  $\beta = 3.9$ . Our sample contains twice as many SNRs as that of Arbutina et al. (2004) and the obtained slope is slightly steeper. Our slope for SNRs in dense ISM is in good agreement with the result obtained by Urošević et al. (2010) for the sample of 31 SNRs in the M82 galaxy ( $\beta = 3.9$ ). Urošević et al. (2010) proposed their relation to be used for estimating distances to SNRs that evolve in a denser interstellar environment, with number density up to  $1000 \text{ particles cm}^{-3}$ . This agreement may be very useful because this is the best sample for the  $\Sigma$ - $D$  analysis, consisting of a relatively high number of very small and very bright SNRs from starburst galaxy M82.

In contrast to the sample of SNRS evolving in a dense environment, we still have a very small sample of SNRs in a low-density medium (Balmer-dominated), consisting of five

SNRs only. Obviously, this sample is too small for any firm conclusions to be made. The  $\Sigma$ - $D$  slope  $\beta = 3.5$  obtained for this sample is close to that for SNRs in a dense environment, and these two classes of SNRs approximately lie on two parallel tracks or domains in the log-log plane, one above another, as expected. However, the small number of objects in the Balmer-dominated sample strongly constrain the reliability of this relation, therefore it should be used with caution. More optical and X-ray observations are needed for discovering new Balmer-dominated (Ia) and oxygen-rich (Ib) SNRs.

We used our new empirical relation to estimate distances to 147 shell-like remnants with unknown distances and obtained a drastically changed the distance scale for Galactic SNRs. Though we are aware of theoretical and statistical flaws in the  $\Sigma$ - $D$  relation, we think that in cases where direct distance estimates are unavailable, the  $\Sigma$ - $D$  relation should remain an important tool for distance determination. The obtained  $\Sigma$ - $D$  relations should be used with caution because uncertainties of distance estimates could be as large as about 50%. Although we have increased the number of calibrators significantly, more observations are needed to get a better understanding of the radio evolution of SNRs. We expect that this paper will potentially be useful for practitioners of radio astronomy, given the improvement expected from future instruments such as SKA.<sup>15</sup>

The authors thank Denis Leahy and Dragana Momić for reading and editing the manuscript. We thank the anonymous referee for useful suggestions that improved the quality of this paper. This work is part of Project No. 176005 “Emission nebulae: structure and evolution” supported by the Ministry of Education, Science, and Technological Development of the Republic of Serbia. B.A. and B.V. also acknowledge financial support through the Projects No. 176004 “Stellar physics” and No. 176021 “Visible and invisible matter in nearby galaxies: theory and observations,” respectively.

*Note added in proof.* After our paper was accepted, we were contacted by Dr. Ping Zhou who pointed out that object Kes 78 actually has an independently determined distance of 4.8 kpc (Zhou & Chen 2011), object 3C391 has another distance estimate of 8 kpc (Chen & Slane 2001 and Chen et al. 2004), and Tycho SNR has a new distance estimate of 2.5 kpc (Zhang et al. 2012). These changes, however, do not significantly affect our results (slope estimates stay within the statistical errors).

## REFERENCES

- Aaronson, M., Bothun, G., Mould, J., et al. 1986, *ApJ*, 302, 536  
 Allakhverdiyev, A. O., Amnuel, P. R., Guseinov, O. H., & Kasumov, F. K. 1983a, *Ap&SS*, 97, 261  
 Allakhverdiyev, A. O., Guseinov, O. H., Kasumov, F. K., & Yusifov, I. M. 1983b, *Ap&SS*, 97, 287  
 Allakhverdiyev, A. O., Guseinov, O. H., & Kasumov, F. K. 1986a, *Afz*, 24, 397  
 Allakhverdiyev, A. O., Guseinov, O. H., Kasumov, F. K., & Yusifov, I. M. 1986b, *Ap&SS*, 121, 21  
 Arbutina, B., & Urošević, D. 2005, *MNRAS*, 360, 76  
 Arbutina, B., Urošević, D., Andjelić, M. M., Pavlović, M. Z., & Vukotić, B. 2012, *ApJ*, 746, 79  
 Arbutina, B., Urošević, D., Stanković, M., & Tešić, Lj. 2004, *MNRAS*, 350, 346  
 Bandiera, R., & Petruk, O. 2004, *A&A*, 419, 419  
 Beck, R., & Krause, M. 2005, *AN*, 326, 414

<sup>15</sup> The Square Kilometre Array will be the world’s largest and most sensitive radio telescope, located in Australia and in Southern Africa, with a total collecting area of one square kilometer.

- Bell, A. R. 1978, *MNRAS*, **182**, 147
- Berezhko, E. G., & Völk, H. J. 2004, *A&A*, **427**, 525
- Berkhuijsen, E. M. 1984, *A&A*, **140**, 431
- Blair, W. P., Sankrit, R., & Raymond, J. C. 2005, *AJ*, **129**, 2268
- Carlton, A. K., Borkowski, K., et al. 2011, *ApJL*, **737**, 22
- Case, G. L., & Bhattacharya, D. 1998, *ApJ*, **504**, 761 (CB98)
- Castelletti, G., Dubner, G., Clarke, T., & Kassim, N. 2011a, *A&A*, **534**, 21
- Castelletti, G., Giacani, E., Dubner, G., et al. 2011b, *A&A*, **536**, 98
- Chen, Y., & Slane, P. 2001, *ApJ*, **563**, 202
- Chen, Y., Su, Y., Slane, P., & Wang, Q.-D. 2004, *ApJ*, **616**, 885
- Chiotellis, A., Schure, K. M., & Vink, J. 2012, *A&A*, **537**, 139
- Clark, D. H., & Caswell, J. L. 1976, *MNRAS*, **174**, 267
- Dragicevich, P. M., Blair, D. G., & Burman, R. R. 1999, *MNRAS*, **302**, 693
- Duric, N., & Seaquist, E. R. 1986, *ApJ*, **301**, 318
- Feldt, C., & Green, D. A. 1993, *A&A*, **274**, 421
- Foster, T., Kothes, R., Sun, X. H., Reich, W., & Han, J. L. 2006, *A&A*, **454**, 517
- Gao, X. Y., Sun, X. H., Han, J. L., et al. 2011, *A&A*, **532**, A144
- Ghavamian, P., Blair, W. P., Sankrit, R., Raymond, J. C., & Hughes, J. P. 2007, *ApJ*, **664**, 304
- Giacani, E. B., Dubner, G. M., Green, A. J., Goss, W. M., & Gaensler, B. M. 2000, *AJ*, **119**, 281
- Giacani, E., Smith, M. J. S., Dubner, G., & Loiseau, N. 2011, *A&A*, **531**, 138
- Giacani, E., Smith, M. J. S., Dubner, G., et al. 2009, *A&A*, **507**, 841
- Gilles, F., & Samar, S. H. 2012, *AdSpR*, **49**, 1313
- Govoni, F., & Feretti, L. 2004, *IJMPD*, **13**, 1549
- Green, D. A. 1984, *MNRAS*, **209**, 449
- Green, D. A. 1991, *PASP*, **103**, 209
- Green, D. A. 2005, *MmSAI*, **76**, 534
- Green, D. A. 2009, *BASI*, **37**, 45
- Green, D. A., Reynolds, S. P., Borkowski, K. J., et al. 2008, *MNRAS*, **387**, L54
- Guseinov, O. H., Ankey, A., Sezer, A., & Tagieva, S. O. 2003, *A&AT*, **22**, 273
- Hayato, A., Yamaguchi, H., Tamagawa, T., et al. 2010, *ApJ*, **725**, 894
- Heng, K. 2010, *PASA*, **27**, 23
- Hewitt, J. W., Rho, J., Andersen, M., & Reach, W. T. 2009, *ApJ*, **694**, 1266
- Isobe, T., Feigelson, E. D., Akritas, M. G., & Babu, G. J. 1990, *ApJ*, **364**, 104
- Jiang, B., Chen, Y., Wang, J., et al. 2010, *ApJ*, **712**, 1147
- Jiang, B., Chen, Y., & Wang, Q. D. 2007, *ApJ*, **670**, 1142
- Junkes, N., Fuerst, E., & Reich, W. 1992, *A&AS*, **96**, 1
- Kothes, R., & Foster, T. 2012, *ApJL*, **746**, 4
- Leahy, D. A., & Tian, W. W. 2007, *A&A*, **461**, 1013
- Li, Z., Wheeler, J. C., Bash, F. N., & Jefferys, W. H. 1991, *ApJ*, **378**, 93
- Lynden-Bell, D., Faber, S. M., Burstein, D., et al. 1988, *ApJ*, **326**, 19
- Mathewson, D. S., Ford, V. L., Dopita, M. A., et al. 1983, *ApJS*, **51**, 345
- McKee, C. F., & Ostriker, J. P. 1977, *ApJ*, **218**, 148
- Milne, D. K. 1970, *AuJPh*, **23**, 425
- Milne, D. K. 1979, *AuJPh*, **32**, 83
- Pacholczyk, A. G. 1970, *Radio Astrophysics* (San Francisco, CA: Freeman)
- Pierce, M. J., & Tully, R. B. 1988, *ApJ*, **330**, 579
- Poveda, A., & Woltjer, L. 1968, *AJ*, **73**, 65
- Reynolds, S. P., & Chevalier, R. A. 1981, *ApJ*, **245**, 912
- Rubin, V. C., Burstein, D., & Thonnard, N. 1980, *ApJL*, **242**, 149
- Sedov, L. I. 1959, *Similarity and Dimensional Methods in Mechanics* (New York: Academic Press)
- Shklovsky, I. S. 1960a, *AZh*, **37**, 256
- Shklovsky, I. S. 1960b, *AZh*, **37**, 369
- Stupar, M., Filipovic, M. D., Parker, Q. A., et al. 2007, *Ap&SS*, **307**, 423
- Strömberg, G. 1940, *ApJ*, **92**, 156
- Tam, C., Roberts, M. S. E., & Kaspi, V. 2002, *ApJ*, **572**, 202
- Tammann, G. A., Loeffler, W., & Schroeder, A. 1994, *ApJS*, **92**, 487
- Tian, W. W., & Leahy, D. A. 2012, *MNRAS*, **421**, 2593
- Uchida, K. I., Morris, M., Bally, J., Pound, M., & Yusef-Zadeh, F. 1992a, *ApJ*, **398**, 128
- Uchida, K., Morris, M., & Yusef-Zadeh, F. 1992b, *AJ*, **104**, 1533
- Uchiyama, Y., Takahashi, T., Aharonian, F. A., & Mattox, J. R. 2002, *ApJ*, **571**, 866
- Urošević, D. 2002, *SerAJ*, **165**, 27
- Urošević, D., Pannuti, T. G., Duric, N., & Theodorou, A. 2005, *A&A*, **435**, 437
- Urošević, D., Vukotić, B., Arbutina, B., & Sarevska, M. 2010, *ApJ*, **719**, 950
- Vink, J. 2012, *A&AR*, **20**, 49
- Xu, J. W., Han, J. L., Sun, X. H., et al. 2007, *A&A*, **470**, 969
- Xu, J.-W., Zhang, X.-Z., & Han, J.-L. 2005, *ChJAA*, **5**, 165
- Zhang, X., Chen, Y., Li, H., & Zhou, X. 2012, *MNRAS*, in press (arXiv:1210.4769)
- Zhou, P., & Chen, Y. 2011, *ApJ*, **743**, 4
- Zhou, X., Yang, C., Yang, S., & Ji, Y. 2009, *ApJ*, **691**, 516